Dynamics of a sleep homeostat observed in glia during behavior

Andres Flores-Valle[1, 2] **and Johannes D. Seelig**[1, *]

[1]Max Planck Institute for Neurobiology of Behavior – caesar (MPINB), Bonn, Germany
[2]International Max Planck Research School for Brain and Behavior, Bonn, Germany
[*]johannes.seelig@mpinb.mpg.de

ABSTRACT

An animal's need to sleep grows with time spent awake and decays again during sleep. In the brain, a homeostatic process or signal has been proposed to represent sleep need, steadily increasing during wakefulness and gradually decreasing during sleep[1,2]. However, such dynamics of a sleep homeostat, capturing the changing need to sleep in real time depending on behavior, has so far not been observed in identified cells[3–6].
Here, using a system that we developed for monitoring calcium activity over multiple days in head-fixed, walking fruit flies[7,8], we find that a class of glia in the fly brain, called ensheathing glia[9–11], shows dynamics expected of a sleep homeostat. Calcium levels in these cells – monitored in a central brain area important for memory, navigation and sleep – integrate activity during wakefulness, reset during sleep, and saturate under sleep deprivation. Optogenetic activation of ensheathing glia induces sleep consistent with charging of the homeostat.
The dynamics of the sleep homeostat, observed in glia of different brain compartments with similar but distinct dynamics, agree with conceptual model expectations[1,2,12,13]. Ensheathing glia therefore act as a system for sleep control distributed across brain areas. The structural arrangement of these glia suggests that sleep homeostasis differentially impacts large ensembles of cells at the same time.

Sleep is important for a number of processes in the brain, many of which are related to plastic changes, such as learning and memory or clearing of waste products[4,14,15]. *Vice versa*, the experience during wakefulness, in particular the duration of time spent awake, but also for example learning or injury, impact subsequent sleep across species[4,15]. However, how neural circuits in the brain integrate the time spent awake as well as specific behaviors for homeostatic sleep regulation, is little understood[3–6].

Regulation of sleep has been conceptually described with the two-process model[1,2]. In this model, a homeostatic process continually increases up to a saturation level during wakefulness, keeping track of an animal's growing need to sleep. Once a threshold of sufficient sleep pressure is reached, the homeostat triggers sleep. During sleep, the homeostat monitors the time spent sleeping by gradually resetting and triggers awakening upon reaching a lower threshold. Both, increase and decrease of the homeostat are describe by exponential dynamics[1,12,13].

In the two-process model, the homeostatic process works together with a second circadian process that depends on the time of day and modulates the upper and lower thresholds at which the homeostat triggers sleep[1,2]. While circadian modulation has been characterized in detail across species[16–18], homeostatic activity has been more difficult to observe[3]. In particular, while recent experiments in mice and fruit flies take advantage of methods for monitoring activity in identified cell types[19–25], the key features of a sleep homeostat, to exponentially approach upper and lower thresholds during epochs of wake and sleep[1,12,13], have so far not been observed.

In *Drosophila*, a number of cell types and brain regions have been found to be important for sleep. Neural substrates for sleep regulation circuits as postulated by the two-process model have been investigated in the ellipsoid body (EB) and fan-shaped body (FB) of the central complex[14,19–21,26,27], an area in the center of the fly brain also important for memory and navigation[28]. Sleep depriving flies for 6[21] or 12[19] hours led to an increase of activity in calcium or electrophysiology recordings in brain explants, consistent with the behavior of a homeostat. Related

observations were also reported in astroglia in fly brain explants, where 12 hours of sleep deprivation led to an increase in calcium fluctuations[25].

However, in flies, sleep processes occur at the timescale of minutes[29,30], with 5 minutes being a frequently used threshold for defining sleep[31], and many short bouts of sleep, lasting minutes to tens of minutes, are distributed throughout the day and night[32–34]. Whether and how the time course of sleep homeostatic signal that is measured after many hours of sleep deprivation[19,21] allows keeping track of such much shorter intervals critical for wake and sleep[32–34] is not known. This motivates experiments in behaving animals where neural activity and behavior are recorded at the same time and which therefore do not have to rely on extended periods of sleep deprivation. For this purpose, we developed methods for imaging in head-fixed walking flies[7], including an approach for correction of axial brain motion during volumetric multiplane imaging[8], that allow combined neural and behavior recordings over multiple days while the fly is maintained in the VR setup.

In mice, calcium imaging in behaving animals was used for investigating sleep regulation in particular with respect to astrocytes[35,36], and calcium signals in freely walking as well as tethered walking animals depended on sleep or wake states, as well as on sleep deprivation[22–24], without however revealing an exponential dependence on behavioral state as expected of a sleep homeostat.

Little is known about the dynamics of glia during behavior in *Drosophila*[37]. Glia constitute about 10 percent of the cells in the fly brain and about 27 percent of these glia are ensheathing glia[9]. Ensheathing glia share similarities with mammalian astrocytes for their role in removing neural debris[10,11,38–42]; they further isolate neural tracts and brain compartments and in that respect are similar to oligodendrocytes[39,43]. Removal of the excitatory amino acid transporter 2 (Eaat2) from ensheathing glia increases sleep[11,44], thus indicating a role of these cells in sleep regulation.

Here, using two-photon calcium imaging[45] over multiple days in head-fixed walking flies, as well as optogenetics in freely walking flies, we show that ensheathing glia monitor sleep and wake, in a behavior dependent manner, in central brain areas with the expected exponential dynamics of a sleep homeostat. We further show that optogenetic activation of glia is sufficient to induce sleep by charging the homeostat. Therefore, ensheathing glia act as a system of sleep control distributed across brain areas.

Glia activity monitors active and rest states

Flies walked on an air supported ball in a virtual reality setup in closed-loop with a single dark stripe on a bright background during the day, and in darkness during the night (12 hours light/dark cycle)[7]. Flies were fed without interrupting the experiments using an automated feeder every 4 hours (Fig. 1a)[7]. We expressed the calcium indicator jGCaMP8m[47] in ensheathing glia using the GAL4 line R56F03[9,48] and imaged in the EB and FB (Fig. 1b,c) as well as the lateral accessory lobe (LAL, Extended Data Fig. S1a), a neuropil associated with the central complex.

Ensheathing glia in EB, FB and LAL showed slow calcium fluctuations that changed together with the animal's walking activity (Fig. 1d, Extended Data Figs. S2-S6a, S1b and Supplementary Videos S1-S6). To determine whether the overall trend of these fluctuations was consistent with the dynamics of a sleep homeostat, we subdivided the fly's behavior in active and rest epochs as defined below.

Walking flies show a distribution of bouts of rest or immobility of different lengths during the day and night[32,33,49,50]. While a frequently used definition of sleep assumes at least 5 minutes of immobility[31,50], already shorter periods of rest show characteristics of sleep with reduced responsiveness to stimuli after 1 minute, and steadily decaying responsiveness over the first 10 minutes of sleep[29,34].

All flies showed a distribution of sleep bouts, including bouts lasting longer than 5 minutes (Extended Data Fig. S7), but in a first approach we distinguished only two behavioral states based on the fly's walking activity: 'walk' (fly is walking) and 'stop' (fly is standing still as assessed based on ball velocity, Fig. 1d). We then selected epochs of at least 30 minutes during which the fly was walking most of the time (active, Fig. 1d) or immobile most of the time (rest, Fig. 1d) by thresholding the 'walk density', obtained by low-pass filtering of 'walk' (see Methods and Table S1 for comparison between immobility, rest, and sleep).

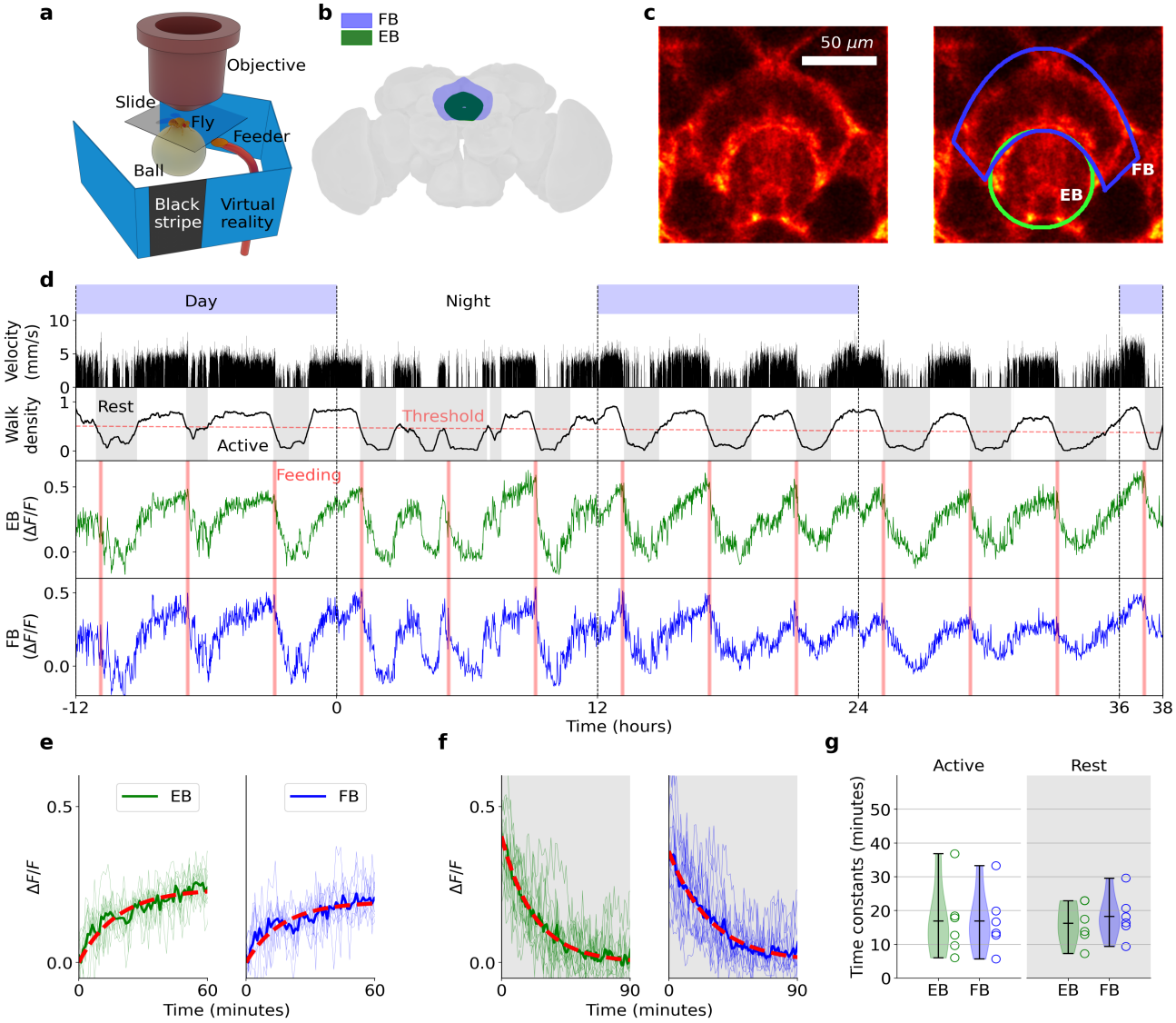

Figure 1. Calcium dynamics in ensheathing glia changes with active and rest states. **a** Setup for long-term imaging: a fly is glued to a cover slide and navigates on an air supported ball in VR under the microscope objective. **b** EB and FB highlighted in the *Drosophila* brain. **c** Left: ensheathing glia express jGCaMP8m. Right: regions of interest (ROIs) for analyzing fluorescence in EB (green) and FB (blue). **d** Long-term recording of a single fly over 38 hours. Top row: day and night cycle in VR. Second row from top: absolute ball velocity. Third row: walk density obtained by low-pass filtering (cut-off period of 0.5 hours) of 'walk' (walk: 1 if the fly has non-zero velocity in 1 second bins, 0 otherwise). Active and rest states were defined when the walk density was above or below a threshold (red line), respectively (see Methods). Fourth and fifth rows: calcium activity (12 hours high-pass-filtered, see Methods) in EB and FB ensheathing glia over time, respectively. Red lines indicate time of feeding. **e** Left side: single traces of increasing calcium activity during active states (thin lines), average (thick line), and exponential fit (red) for EB and FB. Right: same as left but during rest state, fitted with exponentials (red). **g** Time constants for exponential fitting during active (white region) and rest states (grey region) for EB and FB. Violin plots represent distribution of time constants for 6 flies (circles), short horizontal black lines show maximum, mean, and minimum value in descending order. Time constants were not significantly different using t-test ($p > 0.05$).

78 Fluorescence traces were averaged over the selected active and rest epochs and fitted with exponentials (see

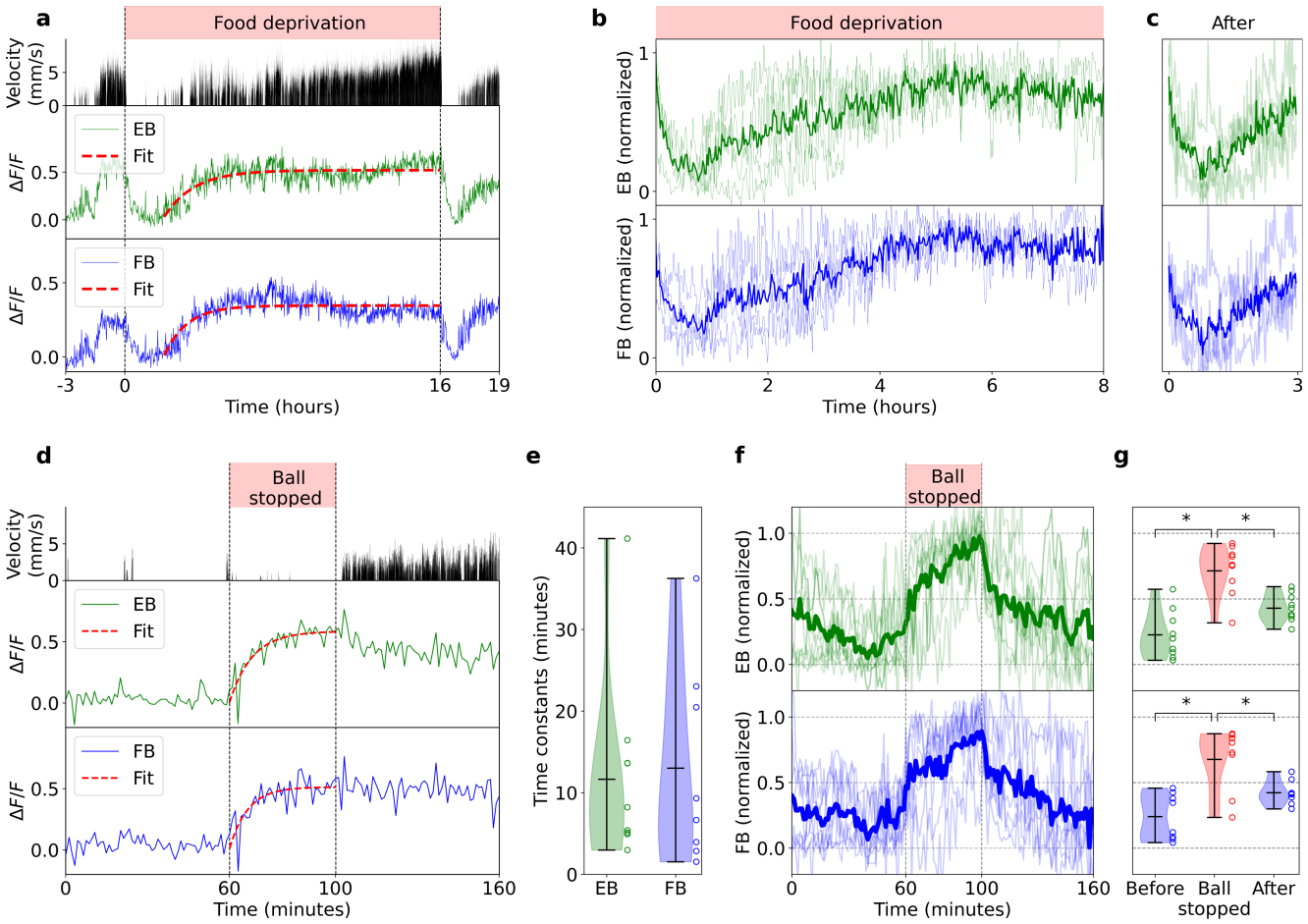

Figure 2. Activity due to sleep deprivation and effort. **a** Behavior and calcium activity in EB and FB ensheathing glia under starvation induced sleep deprivation. Top row: time between two consecutive feeding events (16 hours). Second row: fly velocity. Third and fourth row: activity of glia with exponential fit for visualization of plateau level (red) during food deprivation for EB and FB, respectively. **b** Food deprivation for $N = 4$ flies (including fly in a). Normalized fluorescence traces of ensheathing glia activity in each fly (thin lines) and average (thick line, at least 2 flies) in EB (top) and FB (bottom), respectively, shown during up to 8 hours of food deprivation. Times of food deprivation varied between flies (see Extended Data Fig. S8a-c). **c** Normalized single and average fluorescence traces aligned to first feeding after food deprivation (shown for 3 hours). **d** Calcium activity during effort with blocked treadmill ball. Second row: velocity of fly over time (zero while stopping the ball). Third and fourth row: ensheathing glia activity and exponential fit (red) in EB and FB, respectively. **e** Time constants of exponential fits while ball was stopped for for $N = 10$ trials in 5 flies. **f** Normalized fluorescence traces of activity in EB and FB before, during, and after ball was stopped (top row). Second and thrid row: single trials (thin lines) and average (thick lines) in EB and FB, respectively. **g** Normalized fluorescence levels (y-axis shared with panel f) before, during, and after ball stopping (60, 40, and 60 minutes average), respectively. Asterisks indicate statistical significance for p-values less than 0.05 using t-test.

Methods) the expected time course for homeostatic activity[51,52] (Figs. 1e, f, Extended Data Figs. S2-S6b). The resulting rise and decay time constants for 6 flies for EB and FB, respectively are shown in Fig. 1g (and Table S2). Thus, consistent with the behavior of a sleep homeostat, activity levels changed exponentially on the minutes timescale during epochs where the animals were predominantly active or resting, respectively. Dynamics in the LAL were similar to those observed in EB and FB (Extended Data Fig. S1b).

Wake and sleep behavior was often correlated with feeding (red lines in Fig. 1d, Extended Data Figs. S2-S6a),

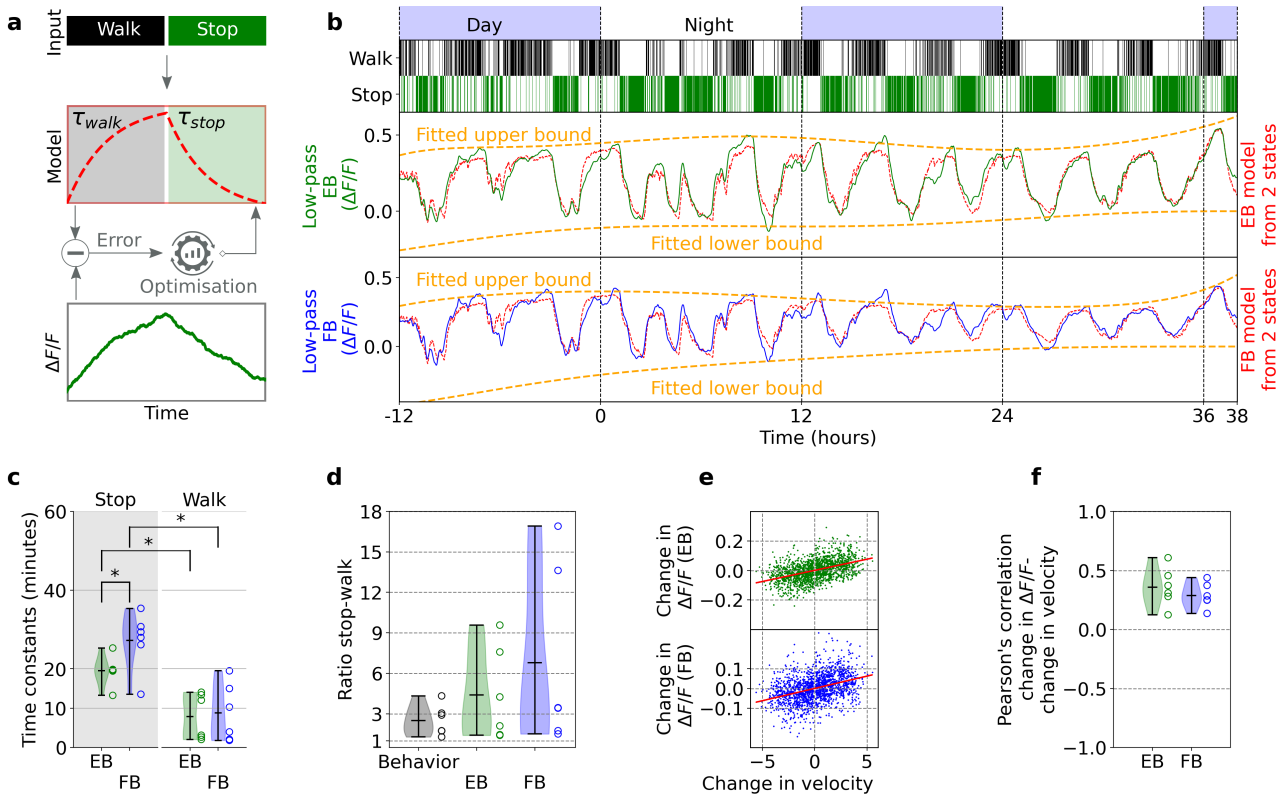

Figure 3. Analysis of slow (two-state model) and fast calcium dynamics. **a** Schematic of model fitting approach: behavior (walk, stop) is integrated as model input with corresponding time constants and fitted to glia activity using optimization. **b** Band-pass filtered (0.5 to 12 hours) calcium activity in EB and FB over time. Top row: 'walk' state (velocity larger than zero in 1 second bins). Second and third row: activity in EB and FB. Red line: fitted homeostat model (two-state model); orange lines: fitted corrections for fluorescence levels (see Methods). **c** Distributions of time constants for 'stop' and 'walk' states from model fitting for $N = 6$ flies in EB (green) and FB (blue). Asterisks represent statistical significance with p-values lower than 0.05 using t-test. **d** Ratios of time in 'stop' and 'walk' states (black) and ratio of time constants between 'stop' and 'walk' state in EB (green) and FB (blue) for each fly ($N = 6$). (Ratios were not significantly different, p-values were above 0.05 using t-test.) **e** Pearson's correlation between changes in high-pass filtered fluorescence changes (ΔF/F) in EB (green) and FB (blue) (see Extended Data Fig. S11) with changes in walking velocity; the red line shows linear fit. **f** Correlation coefficients as in e for $N = 6$ flies. All flies had p-values lower than 0.05 (see Table S3).

with the fly increasingly walking more with time elapsed since feeding and sleeping more after feeding (as observed in freely walking flies[26,53]). However, calcium levels were not correlated with food intake but with walking activity, as seen when the fly walked and stopped independently of feeding, for example after the fourth feeding in Fig. 1d (see Extended Data Figs. S2-S6a for more examples). Additionally, if the fly did not stop walking after feeding, as seen in some instances in Extended Data Fig. S3, calcium levels remained high.

Sleep deprivation saturates glia activity

An expected signature of a sleep homeostat is that it saturates and plateaus under sleep deprivation[1,2]. To verify saturation in ensheathing glia we therefore sleep deprived flies while they were navigating in the VR setup during imaging as described above. Absence of food and starvation induce hyperactivity or foraging behavior and prevent sleep[26,54–56] and in some flies resulted in long epochs of continued fast walking. A walking epoch lasting 16 hours is shown in Fig. 2a. Single trials and average activity of 4 flies that were continuously walking for at least 3 hours following food deprivation with fluorescence traces normalized for comparison, are shown in Fig. 2b (see Extended

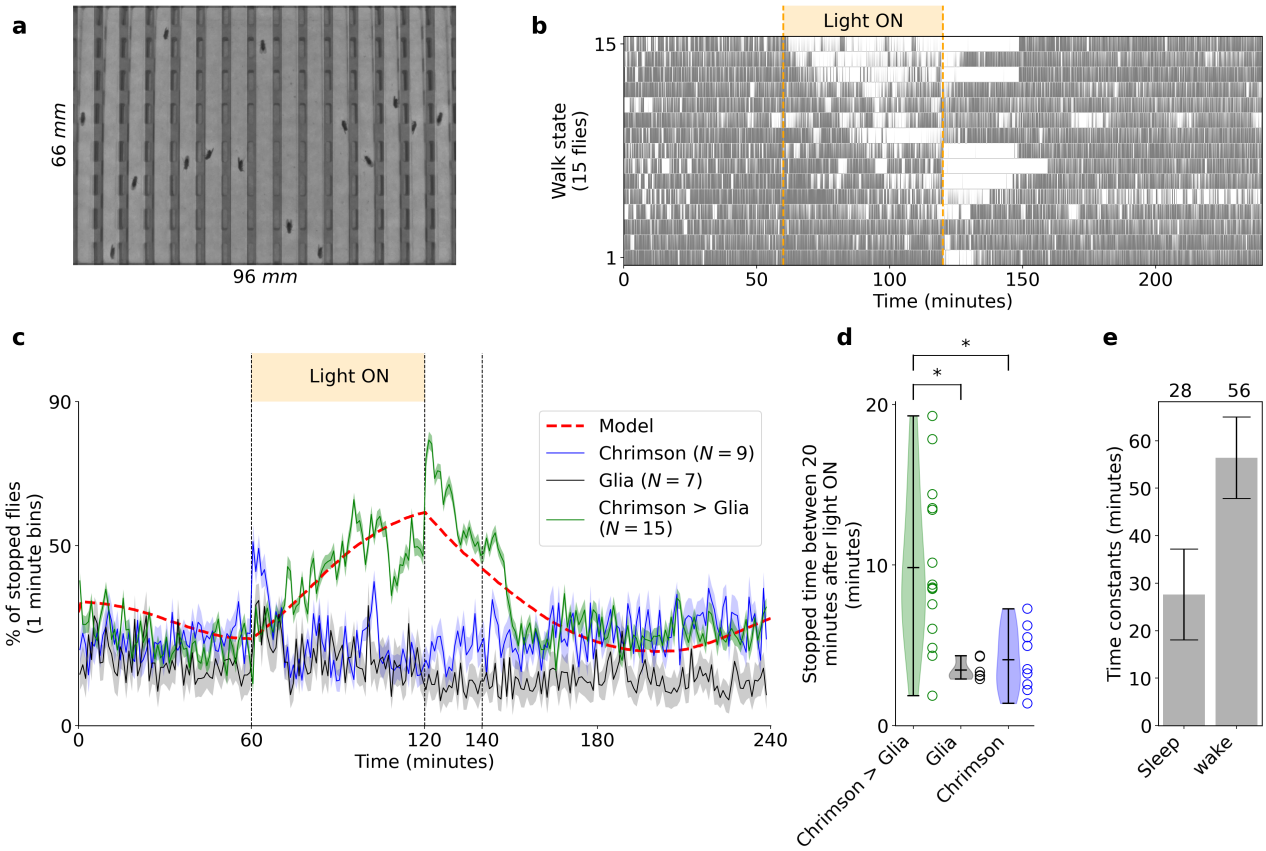

Figure 4. Optogenetic activation of ensheathing glia induces sleep. **a** Top view of sleep monitor used for tracking fly position. Each fly walks in a chamber of 66 mm × 5 mm. **b** Activity (1, if the fly is walking, 0 otherwise) of 15 flies expressing Chrimson in ensheathing glia (UAS-Chrimson-mVenus;R56F03-GAL4) measured during optogenetic activation (top, ordered for visualization according to latency of sleep onset after activation diagonally from top to bottom.)[46]. **c** Proportion of immobile flies over time before, during ('light on'), and after activation for flies expressing Chrimson in ensheathing glia (green line), and control with parents (blue and black lines), red line shows fitted model. Error bands indicate the standard error of the mean (SEM) for each experiment for each 1 minute bin. **d** Immobility during 20 minutes after optogenetic activation (from 120 to 140 minutes) for each fly expressing Chrimson in ensheathing glia (green) and controls (black and blue). **e** Time constants of wake and sleep states of fitted model are shown in c. Error bars indicate fitted standard deviations of time constants (see Methods).

Data Fig. S8a-c for individual traces). Calcium activity after the next feeding following deprivation is shown in Fig. 2c (individual traces again normalized). In some instances, fluctuations around the plateau level (indicated by an exponential fit, red line in Fig. 2a) occurred, often slightly decreasing after long epochs of sleep deprivation, but fluorescence levels nevertheless stayed persistently high.

Using an alternative, mechanical method for sleep deprivation, we periodically touched the fly walking in VR with the tip of a brush mounted on a motorized translation stage. Calcium activity saturated and plateaued similar to starvation induced sleep deprivation, as observed in EB, FB (Extended Data Fig. S8d) and LAL (Extended Data Fig. S1c).

Multiple behaviors induce glia activity

We next asked whether the increase in fluorescence levels in ensheathing glia was specifically due to walking, or whether other effortful behaviors could also cause similar activity changes. To address this question, we immobilized the ball for epochs of 40 minutes while the fly was in the VR setup, and recorded behavior and glia activity.

Movement of the ball was blocked by pushing it against the ball holder with the tip of a brush, positioned close to the fly with a motorized remote controlled micromanipulator during the imaging experiment. This induced the fly to continually push or pull the ball; if the fly stopped moving, the brush was slightly repositioned and, due to the induced perturbation of the ball, the fly resumed active behavior.

As seen in the resulting fluorescence traces and averages in Fig. 2d-g, this led to a steady increase or saturation of calcium levels similar to the dynamics observed due to walking activity (Fig. 1e) with slightly faster time constants (Figs. 2e, 1g). This shows that glia calcium activity increases (Fig. 2g) not only due to coordinated walking but also during other effortful behaviors.

Homeostat model for glia activity

Homeostatic activity is described as exponentially decaying during sleep and exponentially approaching a saturation level during wake[1,51,52]. We therefore quantified whether ensheathing glia integrate behavioral history, that is, wake and sleep, according to such homeostatic dynamics across timescales. For this purpose, we fitted a differential equation with two time constants for charging and resetting of the homeostat, respectively, to ensheathing glia activity dependent on behavioral state (see Methods). As illustrated in Fig. 3a, the behavioral states, for example 'walk' and 'stop', are passed to the model which represents homeostat activity and differentially increases or decreases with time constants characterizing the exponential dynamics. The time constants of the model are fitted to ensheathing glia activity using an optimization approach (see Methods).

In a first homeostat model we did not distinguish between immobility and sleep, but distinguished two behavioral states based on the fly's walking activity for charging and resetting of the homeostat, respectively: 'walk' and 'stop', as defined above (Fig. 3b, Extended Data Figs. S2-S6c).

For model fitting, calcium signals were band-pass filtered to remove fast and slow fluctuations (Fig. 3a, Extended Data Figs. S2-S6c, see Methods). After filtering, slow modulations due to a variety of processes such as photobleaching, potential changes of the preparation due to phototoxicity, or circadian modulation, still need to be taken into account. These changes affect both baseline levels as well as dynamic range of fluorescence signals over time. We therefore fitted two slowly varying envelopes, which corrected for changing dynamic range and baseline, together with the parameters of the homeostat model (yellow lines in Fig. 3b, see Methods).

After fitting, the homeostat model[12,13] describes ensheathing glia activity over the time course of the experiments based on behavior (38 hours in Fig. 3, see also Extended Data Figs. S2-S6 and tables S7, S8 for fit accuracy, and Table S4 for time constants), confirming that ensheathing glia integrate 'walk' and 'stop' states according to the dynamics expected of a homeostat across timescales.

The resulting rise and decay time constants for 6 flies in EB and FB, respectively, are shown in Fig. 3c (see also Extended Data Figs. S2-S6c, e, Table S4). Decay time constants were slower than rise time constants (Fig. 3d) as expected since flies sleep more than they are awake in 24 hours[32,33], different from humans, where the ratio between sleep and wake time constants is about 0.23[12]. Time constants between EB and FB were significantly different during the 'stop' state. Time constants in Fig.1 were more similar between rise and decay than those obtained by model fitting (Fig. 3). This is due to the fact that active and rest states in Fig.1d were determined using low-pass filtering of the animal's walking activity (Fig.1d), thus resulting in rest states that still contained a fraction of walking activity, and *vice versa* for active states.

Models with two different rest states, distinguishing between epochs with less and more than 5 minutes of immobility (defining sleep[31]), were implemented as well, but the time constants for resetting the homeostat between these two rest states were not significantly different, even when defining a sleep state as starting only 5 minutes after the onset of immobility (see Extended Data Figs. S9, S10 and Methods). This shows that the homeostat resets similarly in short and long bouts of immobility, consistent with the observation that already short bouts of immobility show features of sleep[29,34].

Ensheathing glia integrate activity over long timescales (tens of minutes) as indicated by the time constants resulting from model fitting (Table S4). Modulations of fluorescence signals were however already observed at the timescale of 1 minute when comparing changes in walking velocity with changes in high-pass filtered calcium signal ($\Delta F/F$, Fig. 3e, f, Extended Data Figs. S2-S6d, S11, Table S3). Thus, the accumulation of such faster fluctuations

could lead to the integrated activity observed over longer timescales.

Homeostat integrates multiple behaviors

Different behaviors contribute differently to sleep need and are therefore expected to charge the sleep homeostat with different time constants[4,14,26]. We therefore tested whether a more detailed analysis, distinguishing multiple behaviors, could improve model fitting. Behavior on the ball, which was monitored with a camera throughout the experiments, was classified into the following 7 categories using deep learning with 1 second resolution (similar to[57], Extended Data Fig. S14): immobility (stop), proboscis extension, walking, discomfort (where the fly was pushing or pulling the ball), grooming of the front, grooming of the back, and feeding (see Methods and Supplementary Video S7).

Fitting a differential equation similar to the one described above with multiple time constants, requires determining for each behavior whether it charges or resets the homeostat, that is, contributes with a negative or positive weight to the model. This was assessed by selecting all epochs during which the flies continuously showed one behavior over at least two subsequent imaging epochs (summarized for all flies in Extended Data Fig. S12a). As expected (Fig. 1-3), walking as well as pushing and pulling the ball (discomfort) contributed with positive weights, and standing still or sleeping (stop), with negative weights, as indicated by the increasing or decreasing fluorescence signal over epochs of the respective behaviors. Proboscis extension as well as grooming front or back contributed to resetting of the homeostat.

Ensheathing glia calcium signals in EB and FB were fitted to a homeostat model using the classified behaviors (Extended Data Figs. S12b, S2-S6f, Tables S5, S6 and Methods). The resulting time constants for all behaviors and for all flies are shown in Extended Data Fig. S13a. Compared with the 2-state model, the 7-state model resulted in a better fit (Extended Data Fig. S13b), also after accounting for the additional number of fit parameters (see Methods, and Tables S7 and S8). Behaviors that lasted rarely over consecutive imaging epochs, such as discomfort or front or back grooming, contributed with a large uncertainty (as indicated by the large uncertainty of the fit parameters in Extended Data Fig. S2-S6g).

This model predicts that resetting of the homeostat occurs faster during proboscis extension and back-grooming than during immobility, and also resets during front-grooming, although slower than during immobility. Proboscis extension and back-grooming was only observed in short bouts, and rarely over more than two consecutive imaging epochs (Extended Data Fig. S12a). Consistent with this observation, proboscis extension has been described to occur during a deep sleep state, and other brief movements have also been observed during sleep[32,34,49].

Glia activation induces sleep

Based on the described calcium dynamics, we expected that optogenetically activating ensheathing glia should charge the sleep homeostat. This is supported by the observation that modifying membrane transport of ensheating glia by removing Eaat2 modulates sleep[44]. Further, optogenetic activation of astrocytes in sleep related brain areas in mice can induce sleep[58]. We therefore expressed Chrimson[46] in ensheathing glia for optogenetic activation (see Methods). For these experiments, flies walked in elongated chambers and were tracked with a camera under infrared illumination[32,33] (Fig. 4a, b, Supplementary Video S8).

When optogenetically activating the homeostats in a group of flies, different flies will have differently charged homeostats based on their individual sleep and wake histories at the start of the activation period. Additionally, the time constants of the homeostats vary between flies (Figs. 3c and Extended Data Fig. S13a). Based on these two factors, optogenetic illumination will require different times in different flies for saturating the homeostat. Similarly, waking up after saturation of the homeostat will depend on the distribution of the time constants for resetting of the homeostats across flies.

Optogenetic activation of ensheathing glia led to a continuous increase in sleep over time and a decrease of sleep after activation ended (Fig. 4c, d). For interpreting these experiments, we modeled the expected sleep and wake distribution over time (see Methods). For this, we assumed that saturation of the homeostat leads to sleep, and simulated a distribution of initial homeostat levels as well as a distributions of time constants for charging and resetting of the homeostats. The model assumes that optogenetic activation provides an additional input to the

homeostat and therefore leads to a change in time constants, resulting in faster charging during wake and slower decay during sleep (during activation, see Methods). This model was fitted to the observed time course of the sleep and wake distribution before, during, and after activation (red line in Fig. 4c). The time constants resulting from model fitting are shown in (Fig. 4e).

Charging the homeostat optogenetically depends on parameters such as expression levels and on how the resulting currents activate the cells compared with naturally occurring currents. The resulting time constants for charging of the homeostat are therefore expected to be different from those observed in calcium imaging experiments. Additionally, we observed a response to the onset of stimulation light in control flies, as well as an increase in stopped flies right after switching the lights off in Chrimson expressing flies. Thus likely the stimulation light was partially visible for the flies and could therefore contribute to changes in behavior at the onset and offset of the stimulation period.

Time constants for resetting obtained from model fitting were nevertheless comparable to those observed in calcium imaging experiments (Figs. 3c, 4e and Extended Data Fig. S12d). Overall, activating ensheathing glia optogenetically charges the sleep homeostat. Further, the agreement in the time course and time constants between the fitted model and experiments suggests that resetting of the homeostat occurs with similar exponential dynamics in freely walking flies as observed during calcium imaging experiments.

Discussion

Ensheathing glia show the characteristics expected of a sleep homeostat[1,2]: calcium levels increase with behavioral activity during wakefulness, decay when the fly is sleeping (Figs. 1, 3, Extended Data Figs. S12, S2-S6, Supplementary Videos S1-S6), and saturate during sleep deprivation (Fig. 2), all with an exponential time course. The dynamics lie in the behaviorally relevant time range for acting as a sleep homeostat for the sleep bouts in flies which often range from minutes to tens of minutes[32,33,49] with responsiveness to stimuli changing at similar timescales[29,34] (Figs. 1g, 3c, Extended Data Figs. S12d, S2-S6g). Optogenetically activating ensheathing glia induces sleep by charging the homeostat (Fig. 4).

An exponential model for the homeostat[1,12,13] with two time constants for charging and resetting, respectively, dependent on the behavioral state of the animal (two-state model), accurately describes calcium dynamics (Fig. 3, Extended Data Figs. S2-S6). Consistent with the responsiveness to stimuli during rest changing at the minutes timescale[29], this model did not distinguishing rest from sleep based on a threshold of 5 minutes[31,50]. However, models taking that distinction into account (three-state models) yielded similar fits (Extended Data Figs. S9, S10), indicating that the homeostat resets similarly during short and longer epochs of immobility. However, a model differentiating between seven different behavioral states (seven-state model) improved fitting accuracy and indicated variability in charging and resetting dynamics dependent on behavior (Extended Data Figs. S12, S2-S6, Tables S7, S8).

The model time constants were faster for charging than for resetting (Fig. 3c and Extended Data Fig. S13a), consistent with the observation that flies sleep more than they are awake over a 24 hour period[32,33]. The slow calcium decays that continue during long epochs of immobility (Extended Data Fig. S12a, 'stop') show that the fly brain is dynamic during sleep, consistent with previous observations[29,30]. Resetting of the homeostat for example to below 2% from baseline would occur over about 4 time constants, in which case the maximum sleep bouts dependent on the ensheathing glia homeostat would be in the range of 60 to 120 minutes. Longer sleep bouts could for example be controlled by circadian or homeostatic processes occurring on slower timescales[19,21].

The homeostat models were fitted to fluorescence traces of at least 24 hour duration that were filtered to remove fast fluctuations. The models therefore did not capture fluctuations at fast timescales, as observed in the velocity modulations of calcium signals (Fig. 3e, f, Extended Data Figs. S2-S6d and S11). Reaching the upper or lower thresholds of the sleep homeostat did not automatically trigger awakening or sleep onset in head-fixed walking flies, potentially since circadian processes, which according to the two-process model form an oscillating threshold for triggering sleep, were not considered. However, long bouts of activity with a saturated homeostat were only observed under sleep deprivation, due either to hyperactivity induced through food deprivation (Fig. 2a, b) or due to

mechanical perturbation (Extended Data Fig. S8).

Modulation of glia calcium activity during behavior has been observed in a variety of species at different timescales[37], for example modulation dependent on walking velocity in mice[36,59], or integration of behavior over tens of seconds in zebrafish[60]. In head-fixed sleeping flies, a decrease in the fraction of active cells was observed in broad classes of neurons over several minutes[30]. On a similar timescale also metabolic rate decreases during sleep in freely walking flies[61].

Calcium activities monitored in EB, FB, and LAL were qualitatively similar (Extended Data Fig. S1), with however different decay time constants during sleep (Fig. 3c). Ensheathing glia form a barrier around brain compartments[9,43] and could therefore modulate or integrate activity of the underlying circuits. Thus, similarities in the navigation related neural activity between brain compartments in the central complex[28,62,63] could also be reflected in similarities in calcium levels in the respective ensheathing glia. Conversely, differences between ensheathing glia activity in different brain areas would be in agreement with the observation that different behaviors contribute differently to sleep homeostasis[2,4,14,15].

Calcium levels in glia have been suggested as a mechanism for integrating neural activity and providing feedback to underlying neural circuits by modulating their environment[64,65]. Modulation of sleep circuits by glia has for example been described in C. elegans[37,66]. The action of ensheathing glia could include regulation of glutamate in the enclosed circuits[11,67]. In mice, microglia generate inhibitory feedback and suppress activity of glutamatergic neurons[68], a mechanism which could also play a role in sleep regulation[69]. Alternatively, also metabolism or plasticity could be regulated differently between wake and sleep states[64,65]. Removal of neural debris by ensheathing glia after injury is sleep dependent, and thus homeostatic glia activity could also contribute to increased sleep observed under these conditions[41,42]. Potentially ensheathing glia also contribute to structural changes in the healthy brain, similar to astrocytes and microglia in mammals[41,42,70,71]. Such mechanisms, acting similarly across brain compartments, would also be consistent with the observations that ensheathing glia of the LAL (Extended Data Fig. S1), a brain area which has not been associated with sleep circuits, were similarly modulated to those of EB and FB, which contain sleep control circuits[14,20,26].

Combining imaging in behaving flies over long timescales with a range of behavior paradigms, including learning, will enable the investigation of the interplay between sleep homeostasis and sleep function, as well as changes in behavioral state due to circadian modulation or feeding, with the tools available for circuit analysis in the fly.

Funding

Max Planck Society, Max Planck Institute for Neurobiology of Behavior – caesar (MPINB).

Acknowledgements

We thank Marcelo Cintra, Christoph Geisen, Omar Valerio Minero, and Sercan Yegin for help with the MPINB cluster, Ivan Vishniakou for technical support, Tim Krause for preparing fly food, Vivek Jayaraman for Chrimson flies. We thank Kevin Briggman and Jason Kerr for comments on the manuscript.

Author contributions

Both authors designed the study, performed experiments, and wrote the manuscript. AFV performed data analysis.

Competing interests

The authors declare that there are no conflicts of interest related to this article.

References

1. Borbély, A. A. A two process model of sleep regulation. *Hum neurobiol* **1**, 195–204 (1982).

2. Borbély, A. A., Daan, S., Wirz-Justice, A. & Deboer, T. The two-process model of sleep regulation: a reappraisal. *J. sleep research* **25**, 131–143 (2016).

3. Frank, M. G. Challenging sleep homeostasis. *Neurobiol. Sleep Circadian Rhythm.* **10**, 100060 (2021).

4. Duhart, J. M., Inami, S. & Koh, K. Many faces of sleep regulation: beyond the time of day and prior wake time. *The FEBS journal* (2021).

5. Heller, C. The regulation of sleep. In *Oxford Research Encyclopedia of Neuroscience* (2021).

6. Borbély, A. The two-process model of sleep regulation: Beginnings and outlook. *J. Sleep Res.* e13598 (2022).

7. Flores-Valle, A., Honnef, R. & Seelig, J. D. Automated long-term two-photon imaging in head-fixed walking drosophila. *J. neuroscience methods* **368**, 109432 (2022).

8. Flores-Valle, A. & Seelig, J. D. Axial motion estimation and correction for simultaneous multi-plane two-photon calcium imaging. *Biomed. optics express* **13**, 2035–2049 (2022).

9. Kremer, M. C., Jung, C., Batelli, S., Rubin, G. M. & Gaul, U. The glia of the adult drosophila nervous system. *Glia* **65**, 606–638 (2017).

10. Yildirim, K., Petri, J., Kottmeier, R. & Klämbt, C. Drosophila glia: Few cell types and many conserved functions. *Glia* **67**, 5–26 (2019).

11. Bittern, J. *et al.* Neuron–glia interaction in the drosophila nervous system. *Dev. neurobiology* **81**, 438–452 (2021).

12. Borb, A. A. & Achermann, P. Sleep homeostasis and models of sleep regulation. *J. biological rhythms* **14**, 559–570 (1999).

13. Skeldon, A. C., Dijk, D.-J. & Derks, G. Mathematical models for sleep-wake dynamics: comparison of the two-process model and a mutual inhibition neuronal model. *PloS one* **9**, e103877 (2014).

14. Kirszenblat, L. & van Swinderen, B. Sleep in drosophila. In *Handbook of Behavioral Neuroscience*, vol. 30, 333–347 (Elsevier, 2019).

15. Weiss, J. T. & Donlea, J. M. Roles for sleep in neural and behavioral plasticity: reviewing variation in the consequences of sleep loss. *Front. Behav. Neurosci.* 357 (2022).

16. Liang, X., Holy, T. E. & Taghert, P. H. Synchronous drosophila circadian pacemakers display nonsynchronous ca2+ rhythms in vivo. *Science* **351**, 976–981 (2016).

17. Dubowy, C. & Sehgal, A. Circadian rhythms and sleep in drosophila melanogaster. *Genetics* **205**, 1373–1397 (2017).

18. Logan, R. W. & McClung, C. A. Rhythms of life: circadian disruption and brain disorders across the lifespan. *Nat. Rev. Neurosci.* **20**, 49–65 (2019).

19. Liu, S., Liu, Q., Tabuchi, M. & Wu, M. N. Sleep drive is encoded by neural plastic changes in a dedicated circuit. *Cell* **165**, 1347–1360 (2016).

20. Donlea, J. M. *et al.* Recurrent circuitry for balancing sleep need and sleep. *Neuron* **97**, 378–389 (2018).

21. Raccuglia, D. *et al.* Network-specific synchronization of electrical slow-wave oscillations regulates sleep drive in drosophila. *Curr. Biol.* **29**, 3611–3621 (2019).

22. Bojarskaite, L. *et al.* Astrocytic ca 2+ signaling is reduced during sleep and is involved in the regulation of slow wave sleep. *Nat. communications* **11**, 1–16 (2020).

23. Ingiosi, A. M. *et al.* A role for astroglial calcium in mammalian sleep and sleep regulation. *Curr. Biol.* **30**, 4373–4383 (2020).

24. Tsunematsu, T., Sakata, S., Sanagi, T., Tanaka, K. F. & Matsui, K. Region-specific and state-dependent astrocyte ca2+ dynamics during the sleep-wake cycle in mice. *J. Neurosci.* **41**, 5440–5452 (2021).

25. Blum, I. D. *et al.* Astroglial calcium signaling encodes sleep need in drosophila. *Curr. Biol.* **31**, 150–162 (2021).

26. Shafer, O. T. & Keene, A. C. The regulation of drosophila sleep. *Curr. Biol.* **31**, R38–R49 (2021).

27. Flores-Valle, A., Gonçalves, P. J. & Seelig, J. D. Integration of sleep homeostasis and navigation in drosophila. *PLoS Comput. Biol.* **17**, e1009088 (2021).

28. Hulse, B. K. & Jayaraman, V. Mechanisms underlying the neural computation of head direction. *Annu. review neuroscience* **43**, 31–54 (2020).

29. Van Alphen, B., Yap, M. H., Kirszenblat, L., Kottler, B. & van Swinderen, B. A dynamic deep sleep stage in drosophila. *J. Neurosci.* **33**, 6917–6927 (2013).

30. Tainton-Heap, L. A. *et al.* A paradoxical kind of sleep in drosophila melanogaster. *Curr. Biol.* **31**, 578–590 (2021).

31. Huber, R. *et al.* Sleep homeostasis in drosophila melanogaster. *Sleep* **27**, 628–639 (2004).

32. Zimmerman, J. E., Raizen, D. M., Maycock, M. H., Maislin, G. & Pack, A. I. A video method to study drosophila sleep. *Sleep* **31**, 1587–1598 (2008).

33. Donelson, N. *et al.* High-resolution positional tracking for long-term analysis of drosophila sleep and locomotion using the "tracker" program. *PloS one* **7**, e37250 (2012).

34. Van Alphen, B., Semenza, E. R., Yap, M., Van Swinderen, B. & Allada, R. A deep sleep stage in drosophila with a functional role in waste clearance. *Sci. advances* **7**, eabc2999 (2021).

35. Halassa, M. M. *et al.* Astrocytic modulation of sleep homeostasis and cognitive consequences of sleep loss. *Neuron* **61**, 213–219 (2009).

36. Hirrlinger, J. & Nimmerjahn, A. A perspective on astrocyte regulation of neural circuit function and animal behavior. *Glia* (2022).

37. Nagai, J. *et al.* Behaviorally consequential astrocytic regulation of neural circuits. *Neuron* **109**, 576–596 (2021).

38. Doherty, J., Logan, M. A., Taşdemir, Ö. E. & Freeman, M. R. Ensheathing glia function as phagocytes in the adult drosophila brain. *J. Neurosci.* **29**, 4768–4781 (2009).

39. Artiushin, G. & Sehgal, A. The glial perspective on sleep and circadian rhythms. *Annu. review neuroscience* **43**, 119–140 (2020).

40. Lago-Baldaia, I., Fernandes, V. M. & Ackerman, S. D. More than mortar: glia as architects of nervous system development and disease. *Front. Cell Dev. Biol.* **8**, 1527 (2020).

41. Singh, P. & Donlea, J. M. Bidirectional regulation of sleep and synapse pruning after neural injury. *Curr. Biol.* **30**, 1063–1076 (2020).

42. Stanhope, B. A., Jaggard, J. B., Gratton, M., Brown, E. B. & Keene, A. C. Sleep regulates glial plasticity and expression of the engulfment receptor draper following neural injury. *Curr. Biol.* **30**, 1092–1101 (2020).

43. Pogodalla, N. *et al.* Drosophila ßheavy-spectrin is required in polarized ensheathing glia that form a diffusion-barrier around the neuropil. *Nat. communications* **12**, 1–18 (2021).

44. Stahl, B. A. *et al.* The taurine transporter eaat2 functions in ensheathing glia to modulate sleep and metabolic rate. *Curr. Biol.* **28**, 3700–3708 (2018).

45. Denk, W., Strickler, J. H. & Webb, W. W. Two-photon laser scanning fluorescence microscopy. *Science* **248**, 73–76 (1990).

46. Klapoetke, N. C. *et al.* Independent optical excitation of distinct neural populations. *Nat. methods* **11**, 338–346 (2014).

47. Zhang, Y. *et al.* jgcamp8 fast genetically encoded calcium indicators. *Janelia Res. Campus* **10**, 13148243 (2020).

48. Jenett, A. *et al.* A gal4-driver line resource for drosophila neurobiology. *Cell reports* **2**, 991–1001 (2012).

49. Hendricks, J. C. *et al.* Rest in drosophila is a sleep-like state. *Neuron* **25**, 129–138 (2000).

50. Shaw, P. J., Cirelli, C., Greenspan, R. J. & Tononi, G. Correlates of sleep and waking in drosophila melanogaster. *Science* **287**, 1834–1837 (2000).

51. Daan, S., Beersma, D. & Borbély, A. A. Timing of human sleep: recovery process gated by a circadian pacemaker. *Am. J. Physiol. Integr. Comp. Physiol.* **246**, R161–R183 (1984).

52. Borbély, A. A. & Achermann, P. Concepts and models of sleep regulation: an overview. *J. sleep research* **1**, 63–79 (1992).

53. Beckwith, E. J. & French, A. S. Sleep in drosophila and its context. *Front. physiology* 1167 (2019).

54. Lee, G. & Park, J. H. Hemolymph sugar homeostasis and starvation-induced hyperactivity affected by genetic manipulations of the adipokinetic hormone-encoding gene in drosophila melanogaster. *Genetics* **167**, 311–323 (2004).

55. Isabel, G., Martin, J.-R., Chidami, S., Veenstra, J. A. & Rosay, P. Akh-producing neuroendocrine cell ablation decreases trehalose and induces behavioral changes in drosophila. *Am. J. Physiol. Integr. Comp. Physiol.* **288**, R531–R538 (2005).

56. Pool, A.-H. & Scott, K. Feeding regulation in drosophila. *Curr. opinion neurobiology* **29**, 57–63 (2014).

57. Bohnslav, J. P. *et al.* Deepethogram, a machine learning pipeline for supervised behavior classification from raw pixels. *Elife* **10**, e63377 (2021).

58. Pelluru, D., Konadhode, R. R., Bhat, N. R. & Shiromani, P. J. Optogenetic stimulation of astrocytes in the posterior hypothalamus increases sleep at night in c57 bl/6j mice. *Eur. J. Neurosci.* **43**, 1298–1306 (2016).

59. Nimmerjahn, A., Mukamel, E. A. & Schnitzer, M. J. Motor behavior activates bergmann glial networks. *Neuron* **62**, 400–412 (2009).

60. Mu, Y. *et al.* Glia accumulate evidence that actions are futile and suppress unsuccessful behavior. *Cell* **178**, 27–43 (2019).

61. Stahl, B. A., Slocumb, M. E., Chaitin, H., DiAngelo, J. R. & Keene, A. C. Sleep-dependent modulation of metabolic rate in drosophila. *Sleep* **40** (2017).

62. Seelig, J. D. & Jayaraman, V. Neural dynamics for landmark orientation and angular path integration. *Nature* **521**, 186–191 (2015).

63. Lyu, C., Abbott, L. & Maimon, G. Building an allocentric travelling direction signal via vector computation. *Nature* **601**, 92–97 (2022).

64. Frank, M. G. The role of glia in sleep regulation and function. In *Sleep-Wake Neurobiology and Pharmacology*, 83–96 (Springer, 2018).

65. Araque, A. *et al.* Gliotransmitters travel in time and space. *Neuron* **81**, 728–739 (2014).

66. Katz, M., Corson, F., Iwanir, S., Biron, D. & Shaham, S. Glia modulate a neuronal circuit for locomotion suppression during sleep in c. elegans. *Cell reports* **22**, 2575–2583 (2018).

67. Otto, N. *et al.* The sulfite oxidase shopper controls neuronal activity by regulating glutamate homeostasis in drosophila ensheathing glia. *Nat. communications* **9**, 1–12 (2018).

68. Badimon, A. *et al.* Negative feedback control of neuronal activity by microglia. *Nature* **586**, 417–423 (2020).

69. Pfeiffer, T. & Attwell, D. Brain's immune cells put the brakes on neurons (2020).

70. Bellesi, M. *et al.* Sleep loss promotes astrocytic phagocytosis and microglial activation in mouse cerebral cortex. *J. Neurosci.* **37**, 5263–5273 (2017).

71. Deurveilher, S., Golovin, T., Hall, S. & Semba, K. Microglia dynamics in sleep/wake states and in response to sleep loss. *Neurochem. Int.* **143**, 104944 (2021).

72. Huang, C. *et al.* Long-term optical brain imaging in live adult fruit flies. *Nat. communications* **9**, 1–10 (2018).

73. Vishniakou, I., Plöger, P. G. & Seelig, J. D. Virtual reality for animal navigation with camera-based optical flow tracking. *J. neuroscience methods* **327**, 108403 (2019).

74. Bushey, D., Tononi, G. & Cirelli, C. Sleep-and wake-dependent changes in neuronal activity and reactivity demonstrated in fly neurons using in vivo calcium imaging. *Proc. Natl. Acad. Sci.* **112**, 4785–4790 (2015).

75. Berry, J. A., Cervantes-Sandoval, I., Chakraborty, M. & Davis, R. L. Sleep facilitates memory by blocking dopamine neuron-mediated forgetting. *Cell* **161**, 1656–1667 (2015).

76. Virtanen, P. *et al.* SciPy 1.0: Fundamental Algorithms for Scientific Computing in Python. *Nat. Methods* **17**, 261–272, DOI: 10.1038/s41592-019-0686-2 (2020).

1 Methods

Drosophila preparation

Flies were reared in an incubator at 25 degrees on the same 12 hour light/dark cycle used during imaging experiments. Between 3 and 8 day old flies expressing jGCaMP8m in ensheathing glia were used for imaging (UAS-jGCaMP8m;56F03-GAL4). Flies were dissected using laser surgery as described in described[7] to insert a transparent window into the cuticle[72]. The cut cuticle and air sacks were removed under a dissection microscope using forceps, either manually or with a microrobotic arm[7]. The opening was sealed with a drop of transparent UV glue (Freeform, UV fixgel composite). Between 2 and 5 flies were dissected at a time and were left to recover in vials with food for 1 to 3 days before imaging. Flies were then glued to a glass slide using UV glue and transferred to the long-term imaging setup. Flies were selected for imaging based on the optical access to the structures of interest which varied dependent on dissections. Only data recorded at least 48 hours after surgery was included in the analysis.

For optogenetics, flies expressing in ensheathing glia (UAS–mVenus;56F03-GAL4) were transferred to vials with retinal food after hatching. Retinal food was made by adding $20\mu L$ of all-trans retinal (ATR) per $10mL$ of standard food. Flies for control experiments (UAS-Chrimson-mVenus and 56F03-GAL4) were raised without retinal. All flies were maintained in darkness and experiments were performed with 7-8 day old flies.

Imaging setup

The setup for long-term imaging was as described in[7]. For recording volumetric calcium activity and to reduce brain motion artefacts, two axially offset focal planes were recorded at the same time with beams with an extended focal length, with temporally multiplexed acquisition[7]. This setup allowed motion correction at high time resolution in all three dimensions as described in[8]. Fly behavior and virtual reality projection was implemented as previously described[7,73].

Data acquisition

At the start of each long-term imaging experiment, a z-stack of 100 μm depth with axial resolution of 0.25 μm was recorded, which was used for z-motion correction in post-processing[8] (see next section). Additionally, an automated robotic feeder was configured at the beginning of the experiment, which fed flies every 4 hours during 2 minutes[7]. Imaging data was recorded at a resolution of 256×256 pixels at 60Hz for 1 second with a wait time of 60 seconds between consecutive recordings to reduce photobleaching and phototoxicity. The total imaging time was therefore 1.6% of the duration of the experiment. A side view of the fly was recorded with a camera at 10 Hz with a resolution of 640×480 during the whole experiment, which was used later for behavior classification. The VR, implemented as described[27,73] displayed a dark stripe on a bright background using a blue laser (488 nm), which was switched off

during the night for 12 hours. The VR night and day cycle was synchronized to the day and night cycle used in the fly incubator before the experiment. Ball movement was tracked at 200 Hz and a calibration factor for the frame rate and lighting conditions was determined for calculating ball velocities. The temperature of the water perfusing under the objective was 22 degrees[7].

For model fitting, epochs of at least 24 hours were considered (fly 1-6). Flies were left to recover for at least 2 days before imaging started. In flies 1, 2, 5, imaging started after 1 day, but the first day was excluded from data analysis. Food deprivation was performed in flies 2, 4, 5 and 7. Experiments with immobilizing the ball were performed after at least 17 hours of imaging in flies 7, 8, 9, 10. Fly 7 was food deprived during experiments with immobilizing the ball. LAL activity was recorded in flies 5 and 11. Fly 11 was used for mechanical sleep deprivation. Data of fly 1-6 are shown in Figs. 1, 3, Extended Data Figs. S12, S2-S6-S6. Data of fly 2, 4, 5, 7 are shown in Figs. 2a-c and Extended Fig. S8a-c. Data for flies 4, 7, 8, 9, 10 are shown in Figs. 2e-g. Data for fly 5 and 11 are shown in Extended Fig. S1.

Data post-processing

Imaging data was corrected for lateral motion by alignment with respect to a template (average of the first 60 frames) using cross correlation (left in Fig. 1c). The z-stack was also aligned to this template. Then, 24 regions of interests (ROIs) were defined for EB, 24 for FB (Fig. 1c shows the combined ROIs in the EB and FB), and 24 for LAL (in the two flies in Extended Data Fig. S1). The intensity of each ROI was computed by summing all pixel values within each ROI per frame as well as in each frame in the z-stack. The intensity of the ROIs was then used to estimate the z-motion of the sample for each imaging frame as described in[8]. The resulting z-motion over the time of the experiment was filtered using a median filter with 1000 points to discard high-frequency motion, and found maximum displacements of around $10um$ along the z-axis. The filtered z-motion was used to estimate the fluorescence of each ROI corrected from z-motion[8]. Differences between corrected and uncorrected fluorescence was generally low, with maximum differences of 0.1 $\Delta F/F$ due to the extended focal volume used for imaging[8].

Some of the defined ROIs (for example in the center of the EB or FB where expression levels were low) showed only little fluorescence, $F_{ROI}(t)$. We therefore selected ROIs in EB (as well as FB and LAL) with sufficient fluorescence change over time compared to noise, Δ_{ROI}, defined as:

$$\Delta_{ROI} = \frac{SD(F_{ROI}(t))}{SD(N_{ROI})}. \tag{1}$$

Here, $SD(F_{ROI}(t))$ is the standard deviation of the fluorescence in the ROI over time and $SD(N_{ROI})$ is the standard deviation of the expected noise in each ROI. The noise for each ROI was considered to be shot noise, and for a high number of photons detected in each ROI followed a normal distribution with a mean value and standard deviation equal to the average number of photons detected in each ROI (i.e., the average over all imaging frames of the sum of pixel values within each ROI). We therefore selected ROIs with Δ_{ROI} higher than 2, i.e., the change in fluorescence of each ROI needed to be twice that of the expected change due to noise.

Behavior classification

Fly behavior was monitored during the entire experiment using a camera (Extended Data Fig. S14A) under IR illumination at 10 frames per second (fps)[7]. Based on blocks of 10 consecutive frames (1 second time resolution), we classified the following 7 behaviors (rows in Extended Data Fig. S14A): Stop: the fly does not move. Proboscis: the fly does not move but extends and retracts the proboscis. Walk: the fly walks on the ball. Discomfort: the fly pushes or pulls the ball. Grooming front: grooming of head and proboscis with front legs. Grooming back: grooming of the abdomen and wings with hind legs. Feeding: fly is fed with the feeding robot.

We used a 3D convolutional neural network (3D CNN) to classify the behavior based on 10 frames. The field of view of the camera (with resolution 640×480 pixels) was cropped around the fly and was resized to a resolution of $256x256$ pixels. The architecture of the 3D CNN is shown in Extended Data Fig. S14B, where each convolutional block consisted of a 3D convolutional layer with a $3x3x3$ kernel size and rectified linear unit activation function (ReLU), a dropout layer with a rate of 0.2 to prevent overfitting, and 3D max pooling with size $2x2x1$. The filters

of the convolutional layer increased by a factor 2 in each consecutive convolutional block. Finally, a dense layer with a softmax activation function assigned a value to each class. The 3D CNN had a total of around 6.5M trainable parameters.

A total of 45610 manually labeled frames from 10 different flies were used for training. The data was normalized to train the network with the same number of samples for each class. We further increased this dataset with data augmentation that randomly transformed the input frames by changing illumination, translation, rotation and/or scale during training. To train the network we used tensorflow with a binary crossentropy loss function and Adam as optimizer. After 150 epochs with a batch size of 50 samples, the loss function reached a minimum saturation value in about 2 hours, using 4 QUADRO GPUs.

To test the performance of the network, we used 2410 labeled frames, which were augmented to a total of 20000 with the previously described augmentation transformations. The accuracy of the network to predict the right class of behavior was 98.6%, and the normalized confusion matrix for each class is shown in Extended Data Fig. S14C. An example of behavior classification is shown in Supplementary Video S7.

Fitting of fluorescence traces during 'active' and 'rest' states

A commonly used definition of sleep in flies are bouts of quiescence that last at least 5 minutes[31,50], a threshold that has also been used for assessing sleep in tethered walking flies[74,75]. However, shorter bouts of quiescence already show many of the characteristics of sleep[30]. The distribution of bouts of times that the flies did not walk for our experiments is shown in Extended Data Fig. S7. We compare the amount of sleep according to a 5 minutes threshold, according to only distinguishing between walking and stopping, and according to the 'rest' and 'active' states used in Fig. 1 in Table S1. To find epochs of at least 30 minutes during which the fly was walking most of the time (active) or sleeping most of the time (rest), we proceeded as follows: Walking velocity on the ball (with a diameter of 3 mm) was averaged over one second. Velocities below a threshold of 1 mm/s were set to zero to remove tracking noise, and we defined a binary walk state of the fly, $w(t)$, when the thresholded velocity was non-zero ($w(t) = 1$). We defined active and rest states where the fly was walking or standing still most of the time. To calculate these states, we used a walk density, which was defined as alow-pass filter of the walk state with a period of 0.5 hours. Active and rest states were defined based on the walk density being above or below a threshold, respectively (Fig. 1d and Extended Data Figs. S2-S6a). To ensure that the threshold $w_{th}(t)$ was placed centrally between active and rest periods for each fly, it was defined using linear regression to the filtered velocity:

$$w_{th}(t) = at + b, \tag{2}$$

where a and b were fit parameters. A number of N_a fluorescence traces that lasted more than 0.5 hours were obtained during the active epochs, $F^i_{active}(t)$ for $i = 1, ...N_a$. We then selected traces which increased over time, by obtaining the derivative of each trace, $dF^i_{active}(t)$ and computing the ratio between the sum of all positive and the sum of all negative values in the derivative, R^{dF}_{active}, as follows:

$$R^{dF}_{active} = \frac{\sum_t \text{Positive}\left(dF^i_{active}(t)\right)}{\sum_t \text{Negative}\left(dF^i_{active}(t)\right)} \tag{3}$$

If $R^{dF}_{active} > 2$, i.e., if the total positive derivative of each trace was 2 times larger than the total negative derivative, the trace was selected. At least 3 traces were selected for each fly (thin green and blue lines in Figs. 1e, Extended Data Figs. S2-S6b), averaged (thick green and blue lines in Figs. 1e, Extended Data Figs. S2-S6b) and fitted with the following equation:

$$\hat{F}_{active}(t) = A_{active}(1 - e^{-t/\tau_{active}}) + C_{active}. \tag{4}$$

Here, A_{active} is the saturation level of the exponential, C_{active} is an offset and τ_{active} is the time constant. The fit, $\hat{F}_{active}(t)$, is shown in red in 1e and in Extended Data Figs. S2-S6b.

Fly	Sleep using ball velocity (stop) (% per hour)	Sleep using walk density (rest) (% per hour)	Sleep with 5 minutes threshold (% per hour)
1	50.0	49.1	18.7
2	56.8	51.5	28.8
3	68.1	61.0	33.6
4	70.8	51.6	30.4
5	57.6	46.0	19.1
6	76.4	61.2	31.0

Table S1. Percentage of time sleeping per hour for each fly according to the different definitions used in the paper.

Fly	EB		FB	
	τ_{active} (minutes)	τ_{rest} (minutes)	τ_{active} (minutes)	τ_{rest} (minutes)
1	17.8	22.9	16.7	29.6
2	9.6	13.8	5.7	20.7
3	12.7	12.9	13.3	16.4
4	6.0	7.2	12.7	9.3
5	36.8	17.4	33.3	15.5
6	18.4	22.9	19.9	18.1

Table S2. Time constants from fitting exponential curves in the 'active' and 'rest' states for each fly in EB and FB.

Fluorescence traces for the rest state were similarly selected as epochs of at least 0.5 hours during which fluorescence decayed. Decaying traces were selected if the total negative derivative of each trace was 2 times larger than the total positive derivative, i.e., $1/R^{dF}_{rest} > 2$.

All traces (thin green and blue lines in Fig. 1, Extended Data Fig. S2-S6b) were averaged (thick green and blue lines in Figs. 1e and in Extended Data Figs. S2-S6b) and fitted with the following equation:

$$\hat{F}_{rest}(t) = A_{rest} e^{-t/\tau_{rest}} + C_{rest}. \tag{5}$$

Here, A_{rest} is the amplitude, C_{rest} is an offset and τ_{rest} is the time constant of the decay. The fit, $\hat{F}_{rest}(t)$, is shown in red in 1f and in Extended Data Figs. S2-S6b. The time constants during active and rest states in the EB and FB were calculated for a total of 6 flies, and are shown in Fig. 1g and Table S2.

Velocity modulation of glia activity

To assess the influence of fly velocity at short timescales, we computed the mean velocity of the fly during each 1 second imaging epoch, and used a high-pass filter to calculate fluorescence oscillations below periods of 0.5 hours. Extended Data Fig. S11 shows the mean velocity of fly 1 in each trial (black) as well as the high-pass filtered fluorescence in EB (green) and FB (blue). Each data point in Extended Data Fig. S11 was separated by the time

Fly	Number of points	Pearson's correlation (EB)	Pearson's correlation (FB)	p-value (EB)	p-value (FB)
1	1664	0.46	0.37	5.3e-86	3.8e-56
2	1543	0.31	0.25	1.7e-35	4.5e-23
3	680	0.12	0.16	1.2e-03	3.8e-04
4	1065	0.61	0.44	2.1e-108	3.6e-51
5	1283	0.37	0.25	2.3e-43	1.0e-19
6	904	0.28	0.28	1.2e-17	2.9e-18

Table S3. Pearson's correlation between the changes in high frequency fluorescence fluctuations (change in ΔF/F) and changes in velocity.

difference between consecutive imaging recordings of 60 seconds. We computed the change in mean velocity and the change of ΔF/F in EB and FB between consecutive epochs, Fig. 3e and Extended Data Figs. S2-S6d. We fitted a linear regression (red line in Fig. 3e and Extended Data Figs. S2-S6d) and computed the Pearson's correlation between the change in velocity and change in ΔF/F for the EB and FB, finding a positive correlation for each fly with p-values lower than 0.05 (see Fig. 3f and Table S3).

Two-state model of homeostat dynamics

We fitted a differential equation over the time range of each experiment, defined by $[T_{min}, T_{max}]$ for 'stop' and 'walk' periods of the fly. The 'stop' behavior of the fly, $s(t)$, was set to 1 when the velocity of the fly was below a threshold of $1mm/s$ (tracking noise level) and a value of 0 otherwise. Conversely, the 'walk' state of the fly, $w(t)$, was assigned a value 1 for velocities higher than the threshold and 0 otherwise (top row in Fig. 3b and Extended Data Figs. S2-S6c). The time resolution for distinguishing between 'stop' and 'walk' was 1 second. The following model was used for fitting:

$$\dot{h}_v(t) = s(t)\frac{1}{\tau_s}\Big(-h_v(t)+L(t)\Big) + w(t)\frac{1}{\tau_w}\Big(-h_v(t)+U(t)\Big). \tag{6}$$

Here, $h_v(t)$ describes the fluorescence signal ($\Delta F/F$) or homeostat, while $s(t)$ and $w(t)$ act as a binary weights for each behavior. Therefore only one behavioral state contributes to the homeostat at any given time. τ_s and τ_w are the time constants for the stop and walk states, and $L(t)$ and $U(t)$ are functions that describes the lower and upper bounds of the homeostat, respectively. These bounds were allowed to vary with time to take into account slow changes in intensity that are unavoidable during fluorescence recordings over long timescales, such as photobleaching, circadian modulation, or slow changes in calcium levels potentially due to phototoxicity. They were defined as Bezier curves:

$$\begin{cases} U(t) = \sum_k^K C_k u_k \\ L(t) = \sum_k^K C_k l_k, \end{cases} \qquad \text{where} \quad C_k = \binom{K}{k}\left(\frac{T_{max}-t}{T_{max}-T_{min}}\right)^{K-k}\left(\frac{t-T_{min}}{T_{max}-T_{min}}\right)^{k} \tag{7}$$

These curves were fitted at the same time as the parameters of the model. The Bezier curves were parameterized by points separated by at least 6 hours, which defined the number of parameters K for each experiment as

$$K = \lfloor \frac{T_{max}-T_{min}}{6\,\text{hours}} \rfloor, \tag{8}$$

where $\lfloor\cdot\rfloor$ indicates the floor division operation. For each experiment we fitted the 2 time constants τ_s and τ_w, and the K upper and lower bound parameters, u_k and l_k:

$$\{\tau_s, \tau_w, u_1, \ldots, u_K, l_1, \ldots, l_k\}. \tag{9}$$

The fitting procedure is described in the next section. The time constants for the stop and walk states, as well as their estimated errors, were obtained by fitting 2 models (one for EB and one for FB) in each fly, and are shown in Extended Data Figs. S2-S6e and Table S4. The distribution of time constants for each state is shown in Fig 3d where asterisks show statistical significance (p-values lower than 0.05) between the walk and stop states in the EB (green) and FB (blue) using t-test.

Three-state model of homeostat dynamics

In this model we distinguished two states for resetting of the homeostat: a 'stop' state where the fly was at rest (as assessed by ball velocity) for less than 5 minutes, and a sleep state, where the fly was at rest for epochs lasting more than 5 minutes.

$$f(t) = \{\text{Stop}(t), \text{Sleep}(t), \text{Walk}(t)\} \tag{10}$$

Fly	EB		FB	
	τ_{stop} (minutes)	τ_{walk} (minutes)	τ_{stop} (minutes)	τ_{walk} (minutes)
1	25.28 +/- 0.78	12.02 +/- 0.30	35.36 +/- 1.69	10.25 +/- 0.30
2	19.83 +/- 0.59	2.62 +/- 0.07	30.71 +/- 1.18	1.82 +/- 0.04
3	19.43 +/- 0.80	13.39 +/- 0.73	26.12 +/- 1.30	14.98 +/- 0.91
4	13.24 +/- 0.45	3.12 +/- 0.12	13.53 +/- 0.64	3.96 +/- 0.22
5	19.73 +/- 0.75	14.05 +/- 0.69	29.35 +/- 1.61	19.48 +/- 1.22
6	19.52 +/- 1.74	2.04 +/- 0.14	27.95 +/- 3.32	2.05 +/- 0.14

Table S4. Time constants obtained for fitting of 2-state model in each fly.

The following model was used for fitting:

$$\dot{h_s}(t) = \sum_{i}^{N_s} f_i(t) \frac{1}{\tau_i} \Big(-h_s(t) + F(w_i, t) \Big). \tag{11}$$

Here, $h_s(t)$ describes the fluorescence signal ($\Delta F/F$) or homeostat, and $f_i(t)$ acts as a mask for each state, and therefore only the assigned behavior contributes to the homeostat at any given time (similar to the 2-state model). τ_i is a time constant for each behavior i, and w_i is the weight with which each behavior contributes to the homeostat, -1 for 'stop' and 'sleep' states and +1 for 'wake'. F is a function that describes the upper and lower bounds of the homeostat,

$$F[w_i, t] = \begin{cases} U(t) & \text{if } w_i = 1 \\ L(t) & \text{if } w_i = -1, \end{cases} \tag{12}$$

where functions $U(t)$ and $L(t)$ are the upper and lower bounds defined in equation (7), similarly to the previous 2-state model.

For each model we fitted the N_s time constants τ_i and the K upper and lower bound parameters, u_k and l_k:

$$\{\tau_1, ..., \tau_{N_s}, u_1, ..., u_K, l_1, ..., l_k\} \tag{13}$$

An example of the model fitting for EB and FB in fly 1 is shown in Extended Data Fig. S9a. The fitted time constants for each of the states, as well as their estimated errors in EB and FB for fly 1 are shown in Extended Data Fig. S9b. The distribution of time constants for each state in the EB and FB is shown in Extended Data Fig. S9c. Only time constants with an estimated error lower than 0.2 times its fitted value were included to discard estimated time constants with high error. Asterisks in Extended Data Fig. S9c indicate statistical significance (p-values lower than 0.05) between different behaviors in EB (green) and FB (blue) using t-test.

We also asked if the homeostat would reset differently after 5 minutes of immobility. For this purposed we defined a sleep state only after the fly was stopped for 5 minutes and fitted again equation 11. Extended Data Fig. S10a shows an example for EB and FB in fly 1, together with the fitted time constants in Extended Data Fig. S10b. The distribution for time constants with an estimated error lower than 0.2 times its value are shown in Extended Data Fig. S10c for EB and FB. We did not find statistical significance between the time constants of the 'sleep' and 'stop' states using t-test.

Seven-state model of homeostat dynamics

We fitted the dynamics of the homeostat with a model taking into account the $N_b = 7$ classified behaviors from the 3D CNN:

$$b(t) = \{\text{Stop}(t), \text{Proboscis}(t), \text{Walk}(t), \text{Discomfort}(t), \text{Grooming front}(t), \text{Grooming back}(t), \text{Feeding}(t)\} \tag{14}$$

Each behavior, $b_i(t)$, was assigned a binary value, $b_i(t) \in \{0, 1\}$, and only one behavior had value 1 at any given time, corresponding to the maximum class value predicted by the 3D CNN. The time resolution for classification of behavior was 1 second.

Fly	τ_{stop} (minutes)	$\tau_{proboscis}$ (minutes)	τ_{walk} (minutes)	$\tau_{discomfort}$ (minutes)	$\tau_{groomingfront}$ (minutes)	$\tau_{groomingback}$ (minutes)	$\tau_{feeding}$ (minutes)
1	27.84 +/- 2.22	34.04 +/- 8.16	13.79 +/- 0.39	300.00 +/- 129702.72	300.00 +/- 470.43	6.89 +/- 0.51	7.71 +/- 1.45
2	24.46 +/- 1.13	9.99 +/- 1.24	4.36 +/- 0.12	0.03 +/- 0.00	29.74 +/- 4.30	300.00 +/- 1191.49	13.06 +/- 14.37
3	20.35 +/- 1.55	300.00 +/- 1593.52	17.48 +/- 0.93	300.00 +/- 234323.65	28.90 +/- 2.75	9.31 +/- 0.70	4.09 +/- 0.30
4	26.95 +/- 2.46	2.17 +/- 0.16	6.44 +/- 0.41	300.00 +/- 69562.19	22.58 +/- 2.70	5.47 +/- 1.03	4.12 +/- 0.50
5	300.00 +/- 152.64	3.79 +/- 0.42	30.36 +/- 2.42	300.00 +/- 87767.68	17.11 +/- 1.43	22.42 +/- 5.36	300.00 +/- 781.65
6	16.10 +/- 1.66	300.00 +/- 1680.51	3.04 +/- 0.19	300.00 +/- 230055.63	47.81 +/- 17.11	19.33 +/- 8.01	0.34 +/- 0.16

Table S5. Time constants obtained for fitting of 7-state model for EB in each fly.

Fly	τ_{stop} (minutes)	$\tau_{proboscis}$ (minutes)	τ_{walk} (minutes)	$\tau_{discomfort}$ (minutes)	$\tau_{groomingfront}$ (minutes)	$\tau_{groomingback}$ (minutes)	$\tau_{feeding}$ (minutes)
1	27.84 +/- 2.22	34.04 +/- 8.16	13.79 +/- 0.39	300.00 +/- 129702.72	300.00 +/- 470.43	6.89 +/- 0.51	7.71 +/- 1.45
2	24.46 +/- 1.13	9.99 +/- 1.24	4.36 +/- 0.12	0.03 +/- 0.00	29.74 +/- 4.30	300.00 +/- 1191.49	13.06 +/- 14.37
3	20.35 +/- 1.55	300.00 +/- 1593.52	17.48 +/- 0.93	300.00 +/- 234323.65	28.90 +/- 2.75	9.31 +/- 0.70	4.09 +/- 0.30
4	26.95 +/- 2.46	2.17 +/- 0.16	6.44 +/- 0.41	300.00 +/- 69562.19	22.58 +/- 2.70	5.47 +/- 1.03	4.12 +/- 0.50
5	300.00 +/- 152.64	3.79 +/- 0.42	30.36 +/- 2.42	300.00 +/- 87767.68	17.11 +/- 1.43	22.42 +/- 5.36	300.00 +/- 781.65
6	16.10 +/- 1.66	300.00 +/- 1680.51	3.04 +/- 0.19	300.00 +/- 230055.63	47.81 +/- 17.11	19.33 +/- 8.01	0.34 +/- 0.16

Table S6. Time constants obtained for fitting of 7-state model for FB in each fly.

We used the following model to fit the data:

$$\dot{h_b}(t) = \sum_{i}^{N_b} b_i(t) \frac{1}{\tau_i} \Big(-h_b(t) + F(w_i, t) \Big). \tag{15}$$

Here, $h_b(t)$ describes the fluorescence signal ($\Delta F/F$) or homeostat, and $b_i(t)$ acts as a mask for each behavior, and therefore only the assigned behavior contributes to the homeostat at any given time (similar to the 2-state model). τ_i is a time constant for each behavior i, and w_i is the weight with which each behavior contributes to the homeostat, which can take only two values: $w_i \in \{-1, 1\}$. When a weight is $w_i = -1$, the homeostat decreases while the fly performs the behavior, while with $w_i = 1$, the homeostat increases.

F is a function that describes the upper and lower bounds of the homeostat, given by equation (12), similarly to the previous 2- and 3-states model.

To determine the weight of each behavior in the model we used fluorescence traces (EB) from flies that performed one of the 7 behaviors for at least two consecutive imaging epochs (120 seconds). For 'discomfort' we used fluorescence traces recorded when the ball was stopped (Fig. 2f), since this behavior was not observed continuously for 120 seconds when the ball was free to rotate. For the rest of the behaviors we used fluorescence traces from flies 1-6. For each behavior, all traces were aligned at the origin (thin lines in Extended Data Fig. S12a for the EB) and linear regression was used to determine the slope. If the slope was positive for a behavior, the weight was set to 1 and otherwise to -1 (negative slope). We repeated the same procedure for FB and found the same weights as in EB. For each model we fitted the N_b time constants τ_i and the K upper and lower bound parameters, u_k and l_k:

$$\{\tau_1, ..., \tau_{N_b}, u_1, ..., u_K, l_1, ..., l_k\}. \tag{16}$$

Models were fitted independently to EB and FB data.

The fitting procedure is explained in the next section. The time constants for the behavioral states as well as their estimated errors in the EB and FB are shown for each fly in Extended Data Figs. S2-S6g, and Tables S5, S6. Since some behaviors were very rare in some of flies, the estimation error for model fitting was large for some of the time constants. Therefore only time constants with an estimated error lower than 0.2 times its fitted value were included in the distribution of the time constants for each behavior in Extended Data Fig. S13a. Asterisks in Extended Data Fig. S13a indicate statistical significance (p-values lower than 0.05) for behaviors in the EB (green) and FB (blue) using t-test.

Fly	L2 error in 2-state model (EB)	L2 error in 7-state model (EB)	F-statistic (EB)	p-value (EB)
1	3.479988	3.478012	0.32	0.9
2	3.063297	2.696925	70.74	1.1e-16
3	4.955734	4.186857	56.23	1.1e-16
4	4.281183	4.167001	13.01	1.6e-12
5	1.520076	1.658245	-40.54	1.0
6	11.306768	10.176129	61.61	1.1e-16

Table S7. Comparison between 2-state and 7-state models in the EB

Model fitting and comparison

Fitting of models was performed using the function *curve fit* in Scipy[76] in Python. Given a set of initial values of the parameters, we integrated each model with the corresponding equation, for example using equation 6 for the 2-state model, equation 11 for the 3-state model and equation 15 for the 7-state model, from their corresponding states over time, using Euler integration (with 1 second steps). Since the fluorescence data was not recorded continuously, we then interpolated the values of the model in agreement with the times of the recordings. Finally, we obtained an $L2$-error function between the interpolated model values and fluorescence data. The parameter values were updated iteratively from the Jacobian of the error function, and the minimum was found using the trust region reflective algorithm as optimisation method.

To prevent parameters from taking forbidden values during optimisation, we used parameter bounds. For time constants the allowed range was $[0.1, 300]$ minutes, while the allowed range for the upper and lower bound parameters, u_k and l_k, were $[-2, 0]$ and $[0, 2]\Delta F/F$, respectively.

We computed the error or variance of each parameter form the covariance matrix between all parameters, which was returned by the function *curve fit*. This error indicated one standard deviation error of the parameter, obtained as the square root of the corresponding diagonal element in the covariance matrix. In both models, parameters with errors lower than 0.2 times the magnitude of the fitted parameter were considered for distribution analysis (Figs. 3c, S13a).

We compared the 2-state and 7-state models. The 2-state model is a nested model of the 7-state model, meaning that the 2-state model and its parameters are included in the 7-state model and parameters. We therefore asked if a null hypothesis holds, which establishes that the 7-state model does not fit fluorescence data significantly better than the 2-state model. For this purpose we used a F-test. Since the two models have different number of parameters, we can compute the F-statistic of the F-test, as:

$$\text{F-statistic} = \frac{(R_{2-state} - R_{7-state})/(N_{7-state} - N_{2-state})}{R_{7-state}/(N_F - (N_{7-state})}, \tag{17}$$

where $R_{2-state}$ and $R_{7-state}$ are the the residual sum of squares for the 2-state and 7-state model, respectively (same as $L2$-error), $N_{2-state}$ and $N_{7-state}$ are the number of parameters for the 2-state and 7-state model, respectively ($N_{7-state} - N_{2-state} = 5$) and N_F is the number of fluorescence points that was used for fitting both models. The F-statistic value can then be used to generate a p-value, rejecting the null hypothesis stated above if it is lower than 0.05. Since the null hypothesis is rejected, we can conclude that the 7-state model fits the data significantly better.

The L2-errors between each pair of models for each fly in EB and FB are shown in Fig. S13b, while the L2-errors, F-statistic values and p-values comparing each pair of models in EB and FB are shown in Tables S7, S8.

Setup and model for optogenetics

Flies were placed in transparent chambers of 66×5 mm and activity was recorded in up to 15 chamber using a camera from above with a resolution of 1920×1080 pixels running at 30 Hz (Fig. 4a). A rectangular grid of IR LEDs illuminated the chambers from below through a diffuser. A high-pass filter (Thorlabs FGL780S) in front of the camera rejected red light used for optogenetics. Four red LEDs (Thorlabs LED780L), two on each side and outside of the field of view of the camera, illuminated all chambers homogeneously for optogenetics. Activation

Fly	L2 error in 2-state model (FB)	L2 error in 7-state model (FB)	F-statistic (FB)	p-value (FB)
1	3.588580	3.246188	59.59	1.1e-16
2	0.784993	0.733569	36.50	1.1e-16
3	3.402890	2.818227	63.52	1.1e-16
4	1.604965	1.512774	28.95	1.1e-16
5	2.616210	2.554074	11.84	2.4e-11
6	5.747171	5.153419	63.90	1.1e-16

Table S8. Comparison between the 2-state and 7-state models in the FB

was performed with pulses of 20 ms at 1 Hz.Optogenetics experiments lasted for 240 minutes and the red LEDs for optogenetics were activated from minutes 60 to 120 of the experiment.

Tracking of the fly positions was done offline, using color segmentation in OpenCV and Python, by extracting the dark color of the flies from the bright background (Supplementary Video S8). The position and velocity of each fly in its chamber was further smoothed using a Kalman filter. Fig. 4b shows examples of velocity profiles from 3 different flies during the experiment. Three different experiments were performed, one for ensheathing glia expressing Chrimson (UAS-Chrimson-mVenus;R56F03-GAL4) and two controls for each of the parents (UAS-Chrimson-mVenus and R56F03-GAL4). For each experiment we computed the percentage of flies that were stopped in 1 minute bins, shown in Fig. 4c. We computed the total stop time of each fly for each experiment 20 minutes after optogenetic activation (between 100 and 120 minutes), as shown in Fig. 4d, and found statistical significance between the stop distribution among the 3 experiments considering p-values lower than 0.05 with a t-test.

We fitted time constants from a homeostatic model (similar to the 2-state model) to the percentage of stopped flies during the experiment with ensheathing glia expressing Chrimson. We used the following model:

$$\dot{h}(t) = w(t)\frac{1}{\tau_w}\Big(-h(t)+w(t)+w_I I(t)\Big) + [1-w(t)]\frac{1}{\tau_s}\Big(-h(t)+w_I I(t)\Big). \tag{18}$$

Here, $w(t)$ is the wake state of the fly, which has value 1 when a fly is awake and 0 when it is asleep, τ_w and τ_s are the time constants during the sleep and wake states, and $I(t)$ represents an input to the hemostat due to optogenetics, which is set to zero except when the light is ON. The weight w_I represents a weight of the optogenetic contribution to homeostat activity. The state of a fly, $w(t)$, switches from 1 (wake) to 0 (sleep) when the homeostat reaches an upper bound, h_{max}, and switches from 0 to 1 when the homeostat decreases and reaches a lower bound, h_{min}. Therefore the simulated state of a fly at any time, $w(t)$, depends on the homeostat dynamics, $h(t)$. We simulated a total of $N_s = 500$ flies with different homeostats, where the lower and upper bound were randomly drawn from a uniform distribution,

$$\begin{cases} h^i_{min} \sim \mathscr{U}(0.05, \quad 0.2) \quad \text{for } i = 1,...,N_s \\ h^i_{max} \sim \mathscr{U}(0.8, \quad 0.95). \end{cases} \tag{19}$$

Here, $\mathscr{U}(a,b)$ represents a uniform distribution over the interval [a,b]. The time constants of each simulated homeostat, τ^i_s and τ^i_w were drawn from a Normal distribution,

$$\begin{cases} \tau^i_s \sim \mathscr{N}(\hat{\tau}_s, \sigma_s) \quad \text{for } i = 1,...,N_s \\ \tau^i_w \sim \mathscr{N}(\hat{\tau}_w, \sigma_w). \end{cases} \tag{20}$$

Here, $\hat{\tau}_s$ and $\hat{\tau}_w$ are the means and σ_s and σ_w are the standard deviations of the distributions of the time constants for the stop and wake states, respectively. Only values larger than 1 were considered to avoid 0 or negative time constants.

The initial wake state of each simulated fly, $w^i(0)$, was chosen randomly so that the fraction of simulated flies in the wake state was the same as the one at the beginning of the optogenetics experiment (which was about 68%),

while the initial value of each simulated homeostat, $h^i(0)$, was drawn from a uniform distribution between the corresponding upper and lower bound, $h^i(0) \sim \mathscr{U}(h^i_{min}, \quad h^i_{max})$. After computing the homeostat dynamics for each simulation, $h^i(t)$, by solving equation (18) through Euler integration, and obtaining the corresponding wake states for each simulation, $w^i(t)$, we computed the proportion of awake simulated flies at each time, and obtained a $L2$-error with respect to the optogenetics experiment (ensheathing glia expressing Chrimson). This allowed us to minimize the $L2$-error with respect to the following parameters:

$$\{\hat{\tau}_s, \sigma_s, \hat{\tau}_w, \sigma_w, w_I\}. \tag{21}$$

We therefore fitted a normal distribution of the time constants to the sleep and wake states, which is shown in Fig. 4e and the weight for optogenetics (not shown). We fitted all models using the *curve fit* function in the Scipy package in Python, using the trust region reflective algorithm for optimisation. The parameters had lower and upper bounds during fitting: for the mean time constants $\hat{\tau}_s, \hat{\tau}_w \in [0, 300]$ minutes, for the standard deviations of the time constants, $\sigma_s, \sigma_w \in [1, 20]$ minutes and for the optogenetics weights $w_I \in [0, 1]$. The proportion of simulated wake flies with the fitted parameters is shown in red in 4c.

The model considers that optogenetics activation acts as an input to the homeostat, changing the time constants of the dynamics, equation 18, as:

$$\dot{h}(t) = w(t)\frac{1}{\tau_w}\Big(1 + \frac{w_I I(t)}{-h(t) + w(t)}\Big)\Big(-h(t) + w(t)\Big) + [1 - w(t)]\frac{1}{\tau_s}\Big(1 + \frac{w_I I(t)}{-h(t)}\Big)\Big(-h(t)\Big). \tag{22}$$

Separating for sleep and wake yields:

$$\begin{cases} \dot{h}(t) = \frac{1}{\tau_w}\Big(1 + \frac{w_I I(t)}{-h(t)+w(t)}\Big)\Big(-h(t) + w(t)\Big) & \text{when } w(t) = 1 \text{ (wake)} \\ \dot{h}(t) = \frac{1}{\tau_s}\Big(1 + \frac{w_I I(t)}{-h(t)}\Big)\Big(-h(t)\Big) & \text{when } w(t) = 0 \text{ (sleep)} \end{cases} \tag{23}$$

If we consider that the homeostat is fully reset ($h(t) \longrightarrow 0$) at the beginning of the wake state, and fully charged ($h(t) \longrightarrow 1$) at the beginning of the sleep state, the effective time constants for wake and sleep, $\hat{\tau}_w$ and $\hat{\tau}_s$ during optogenetic activation ($I(t) = 1$) are:

$$\begin{cases} \hat{\tau}_w = \tau_w/(1 + w_I) \\ \hat{\tau}_s = \tau_s/(1 - w_I) \end{cases} \tag{24}$$

The fitted value for the optogenetic weight was $w_I = 0.63$. Therefore, optogenetic activation approximately decreased the effective wake time constant of the homeostat by a factor of 0.61, as expected resulting in the homeostat charging faster, while it approximately increases the time constant during sleep by a factor of 2.70, resulting in slower resetting.

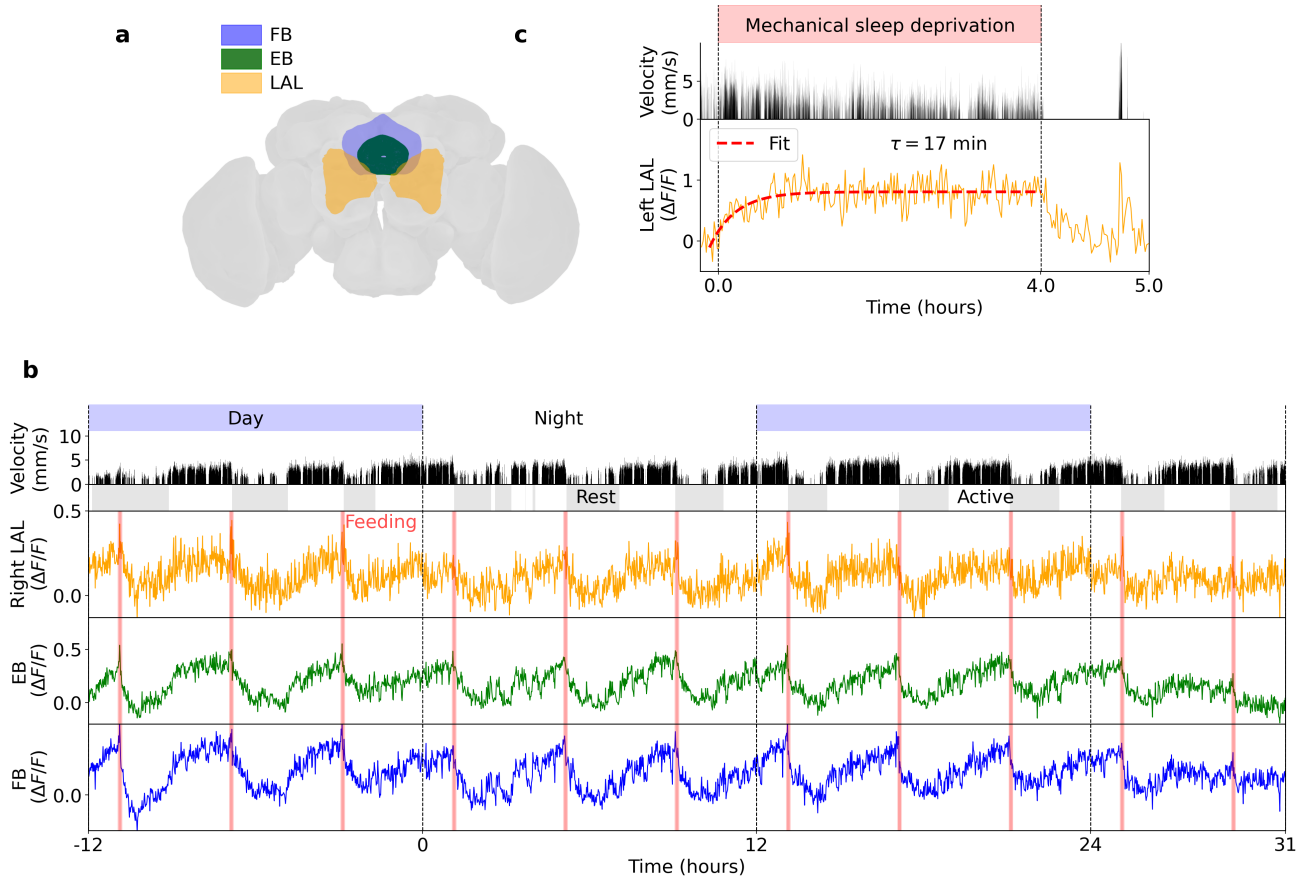

Figure S1. **a** Schematic of EB, FB and left and right LAL regions in the fly brain. **b** Activity of LAL, EB and FB over time (fly 5). First row shows day and night cycle in VR, second row shows fly velocity, third row shows rest (grey areas) and active (white areas) behavioral states. The bottom 3 rows show activity in the right LAL and activity in the EB and FB for comparison, respectively. **c** Mechanical sleep deprivation of fly (top row) walking in VR with velocity shown in the second row and the recorded activity in the left LAL (third row). Sleep deprivation was achieved by periodically touching the fly, which was walking in VR, with the tip of a brush on a automated micromanipulator.

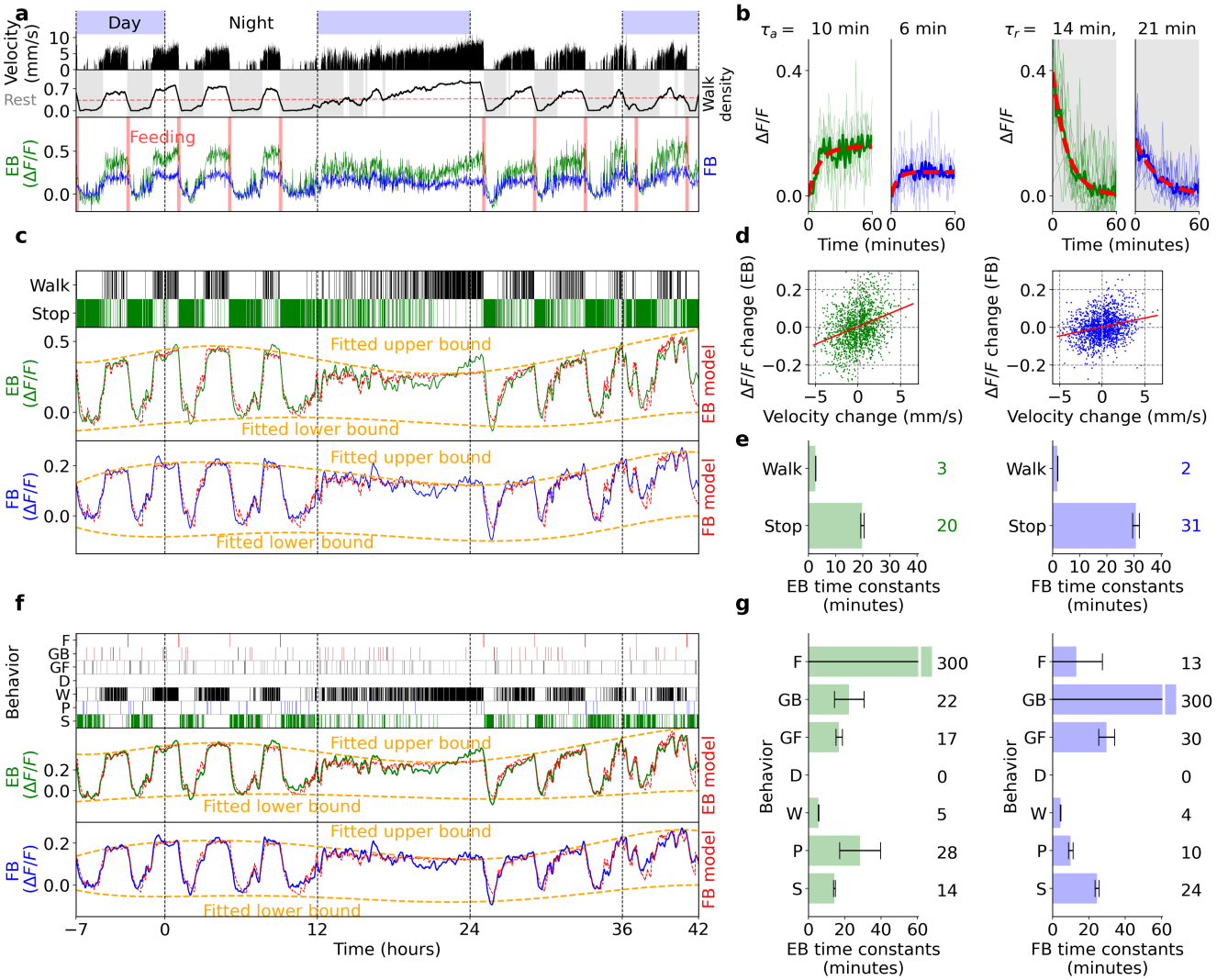

Figure S2. Data and models for fly 2. **a** Glia activity over time (same as Fig. 1d). Top row indicates day and night cycle, second row shows fly velocity, third row shows rest (grey area) and active (white area) states, obtained by thresholding of the walk density (see Methods). Fourth row shows high-pass filtered activity (periods larger than 12 hours are filtered) of glia in the EB (green) and FB (blue). Red vertical bars indicate feeding. **b** Fluorescence traces during active (left) and rest (right) states in EB (thin green lines) and FB (thin blue lines), their averages (thick lines) and an exponential fit (red). **c** 2-state model fitting, same as Fig. 3a. Top row shows walk (black) and stop (white) state of the fly, second and third row show 2-state model fit (red line) with corresponding bounds (orange lines) for band-pass filtered activity in EB and FB, respectively. **d** Correlation between changes in high frequency fluorescence signal, ΔF/F, in EB (left) and FB (right) with changes in velocity. **e** Time constants of 2-state model fitted in panel c for EB (left) and FB (right). **f** 7-state model fit, same as in Fig. S12b. Top row shows classified behavior of the fly over time and second and third rows show 7-state model fit (red line) with corresponding bounds (orange lines) for band-pass filtered activity in EB and FB, respectively. **g** Time constants of the 7-state model fitted in panel f for the EB (left) and FB (right). Bars graphs in e and g visualize numbers shown on the right, error bar indicates the estimated error of each fitted parameter (see Methods). For errors outside of the limits of the plot, the error bar appears as a vertical line.

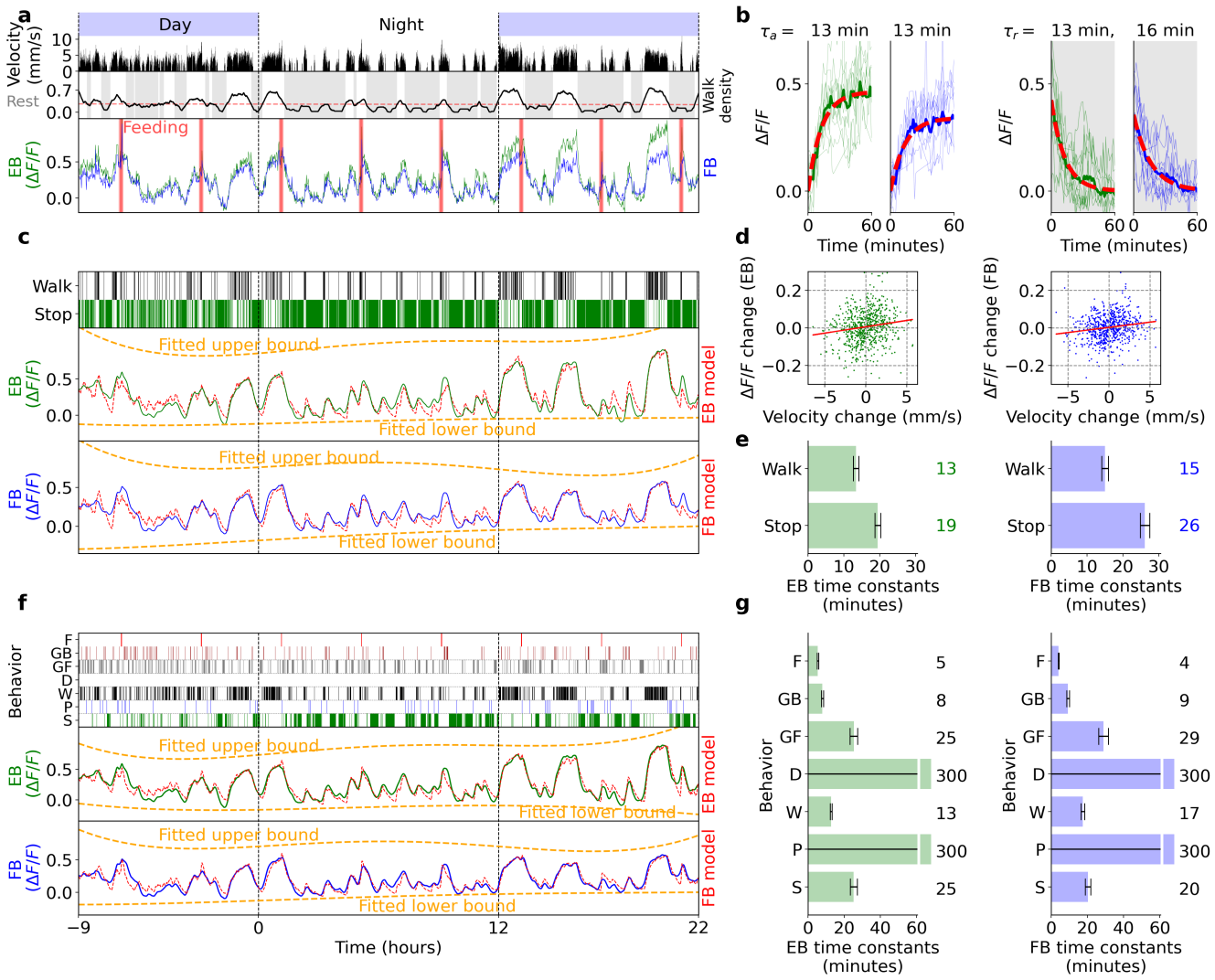

Figure S3. Same as Extended Data Fig. S2 for fly 3.

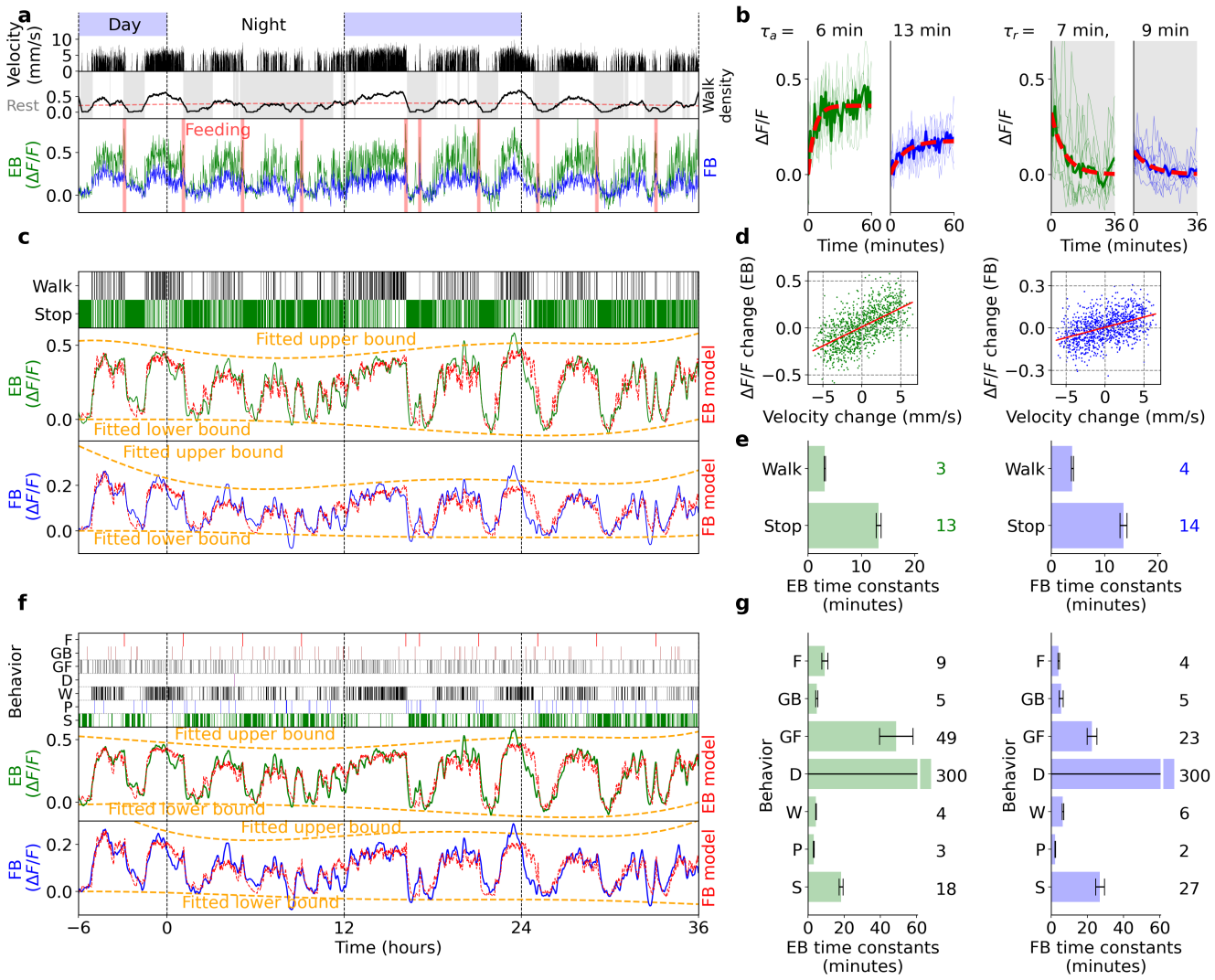

Figure S4. Same as Extended Data Fig. S2 for fly 4.

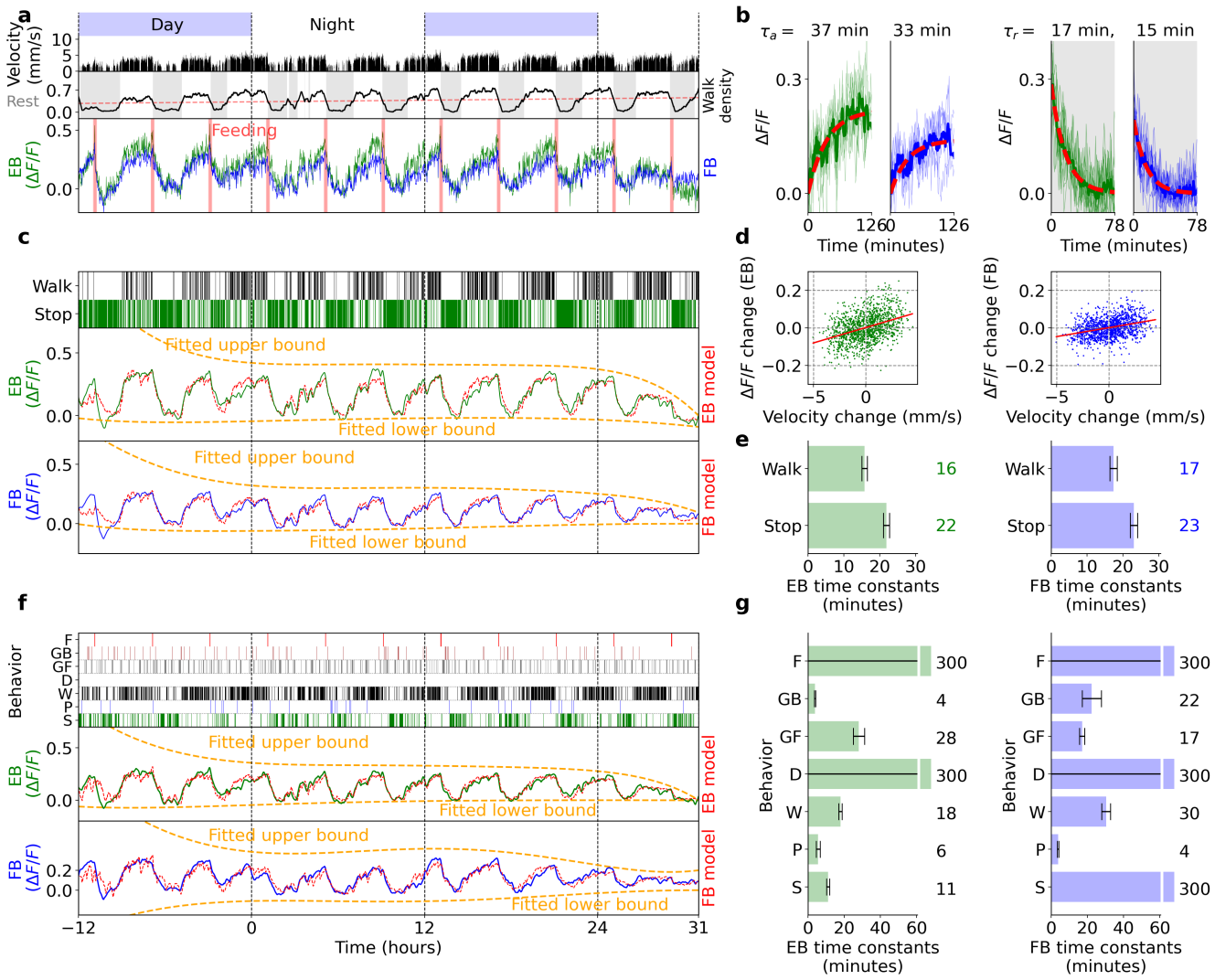

Figure S5. Same as Extended Data Fig. S2 for fly 5.

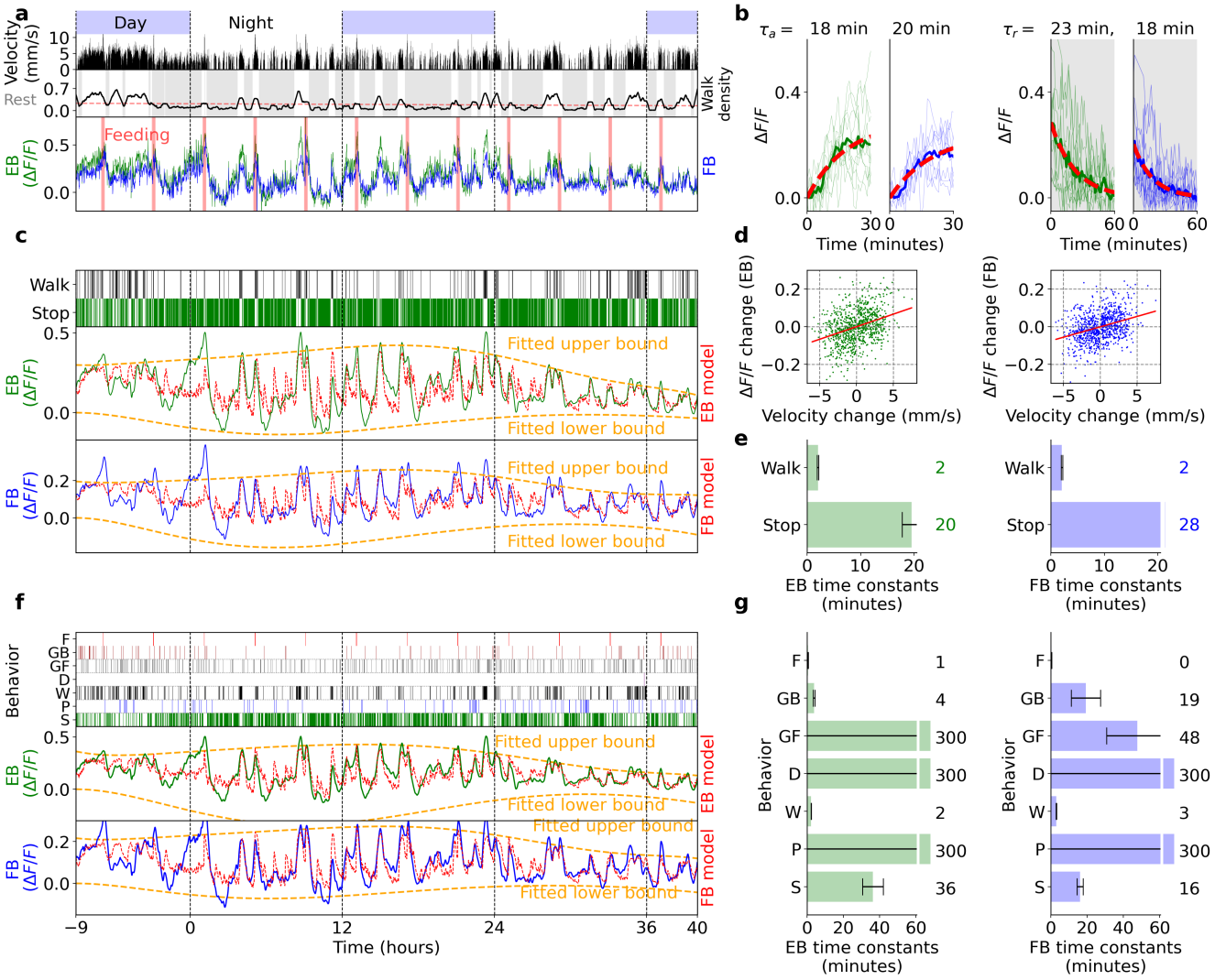

Figure S6. Same as Extended Data Fig. S2 for fly 6.

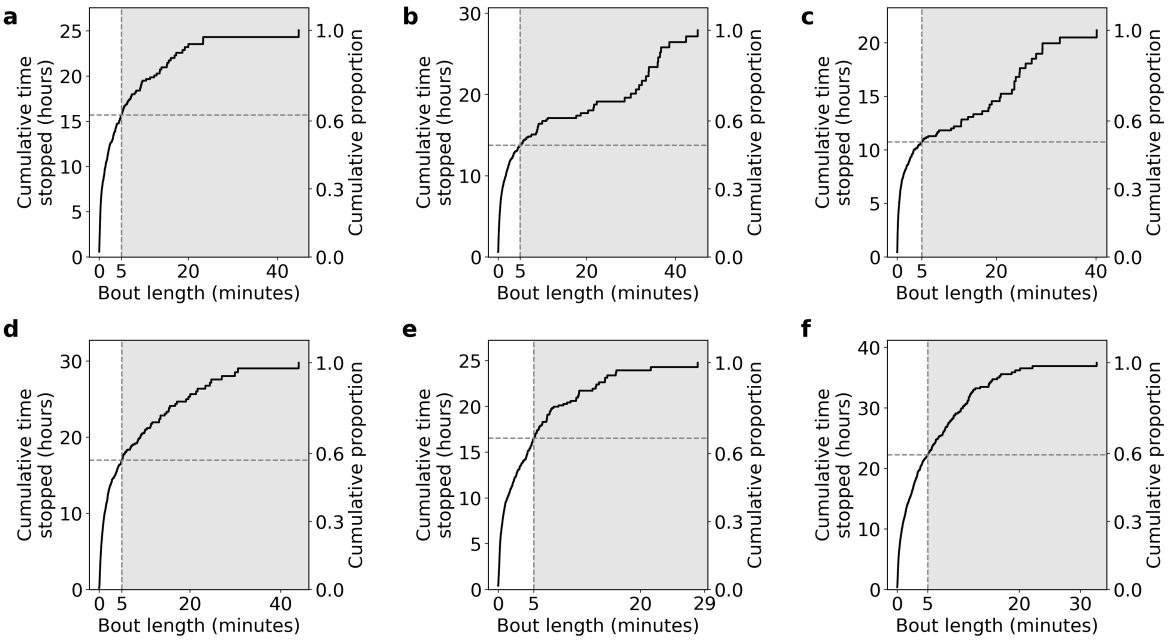

Figure S7. Cumulative time time that each fly stops (left y-axis) and corresponding proportion over the total stop time (right y-axis) as a function of the stop duration (**a**-**f** correspond to flies 1-6). Bouts where the fly stops for less than 5 minutes (white background) correspond to around 0.6 of the total stop time across flies.

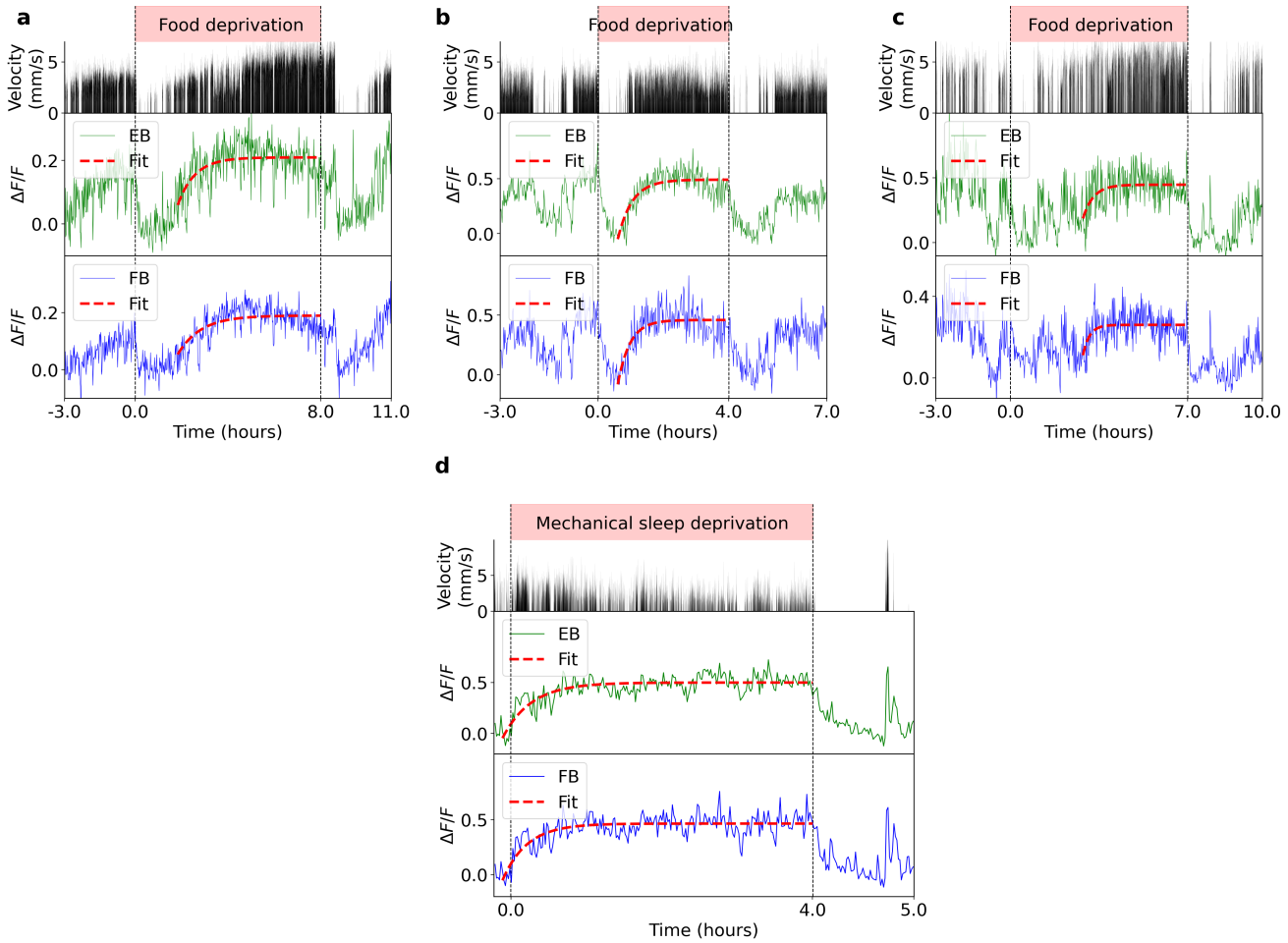

Figure S8. **a-c** Velocity over time (second row) and glia activity in EB (third row) and FB (fourth row) during food deprivation (first row) for 3 different flies. These 3 flies together with the fly in Fig. 2a are summarized in Fig. 2b. **d** Mechanical sleep deprivation of fly walking in VR. Sleep deprivation was achieved by periodically touching the fly with the tip of a brush while it was walking in VR. Exponential fits are shown for visualization of saturation levels.

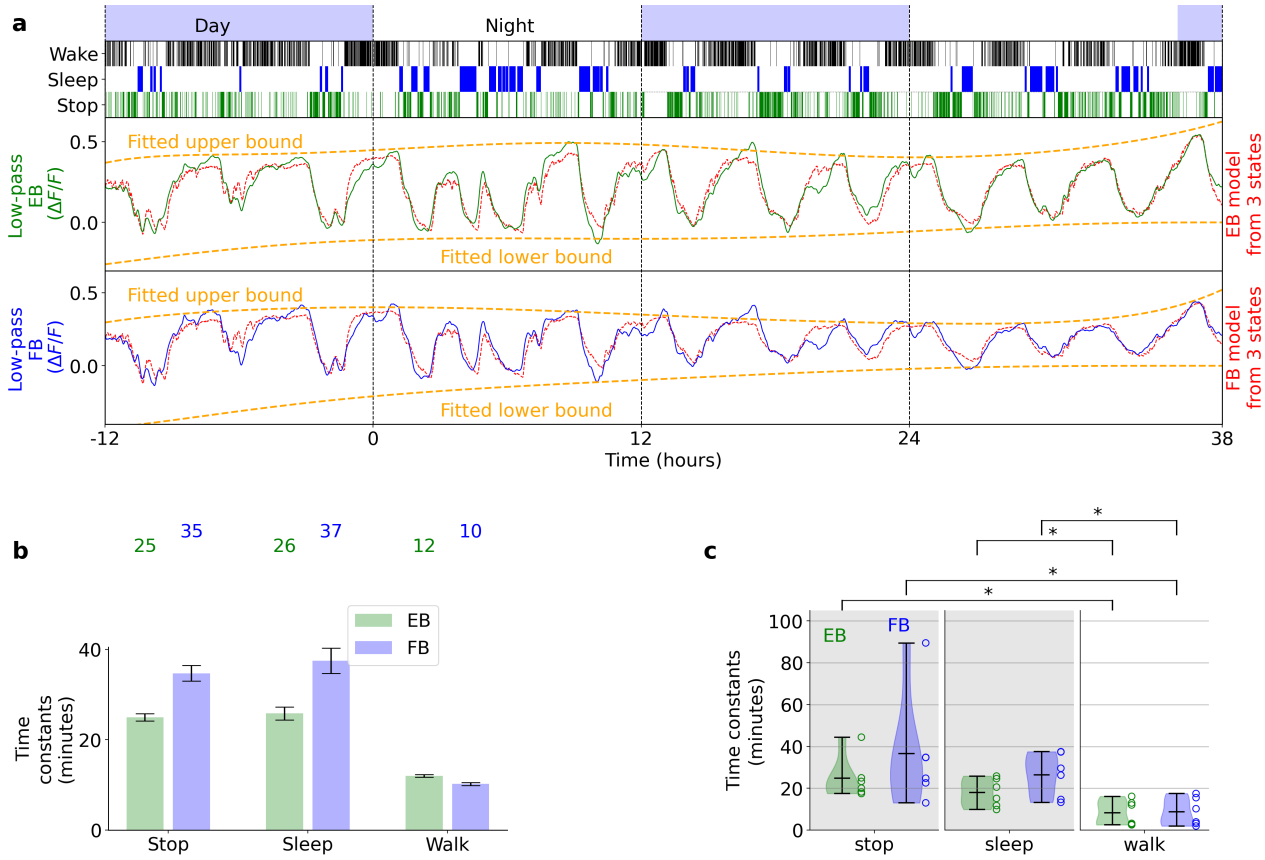

Figure S9. Fitting glia activity with 3-state model defining a 'sleep' state as epochs where the fly was stopped for more than 5 minutes. **a** First row shows day and night cycle in VR, second row shows behavior of fly 1 extracted from ball velocity. Sleep is defined as epochs where the fly stops walking for at least 5 minutes. The third and fourth rows show fitting of the 3-state model (red line) and corresponding bounds (orange lines) in EB and FB, respectively. **b** Time constants of the 3 states resulting from fitting in a for EB (green) and FB (blue). **c** Distribution of time constants for the 3 states for $N = 6$ flies. Asterisks represent statistical significance between states, with p values lower than 0.05 using t-test.

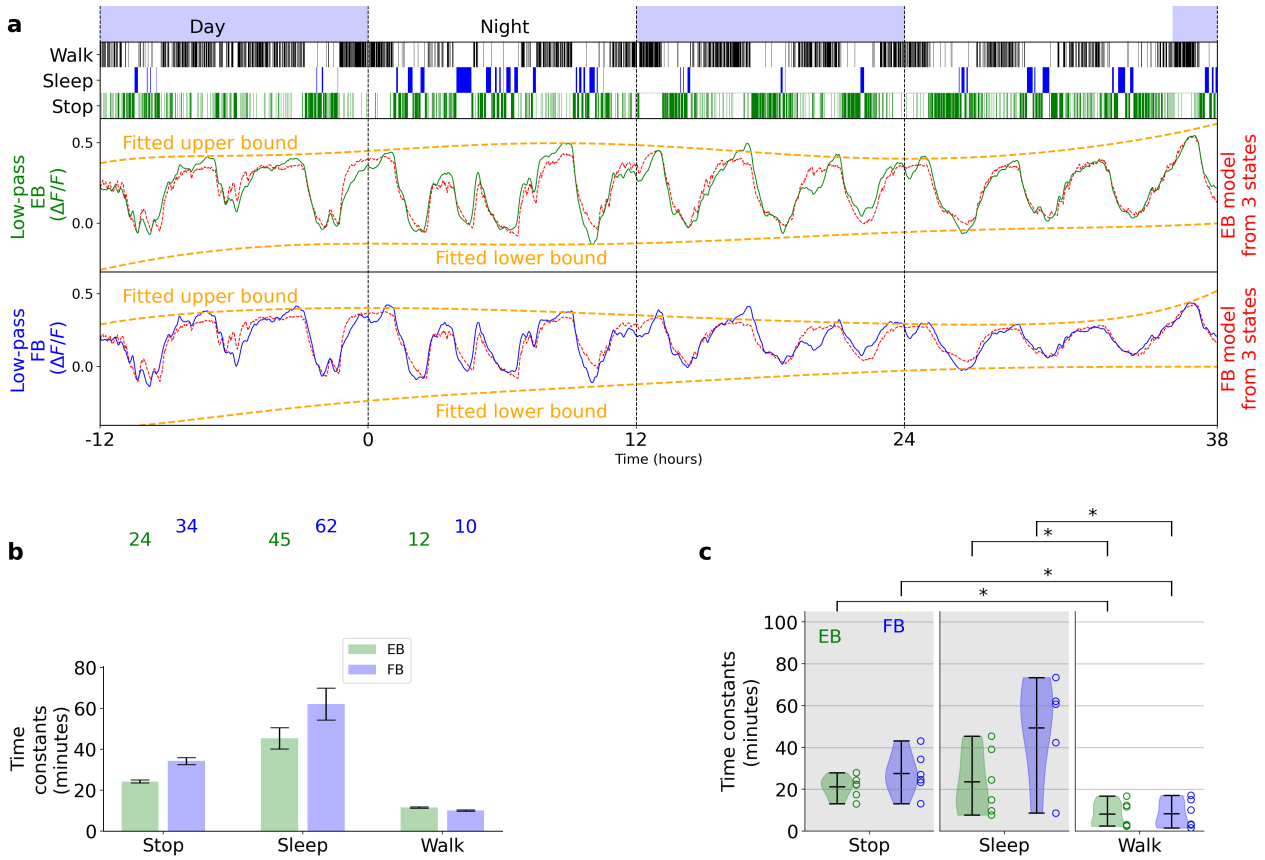

Figure S10. Fitting glia activity with 3-state model with a 'sleep' state define as only after 5 minutes of immobility. Same as Extended Data Fig Fig. S9.

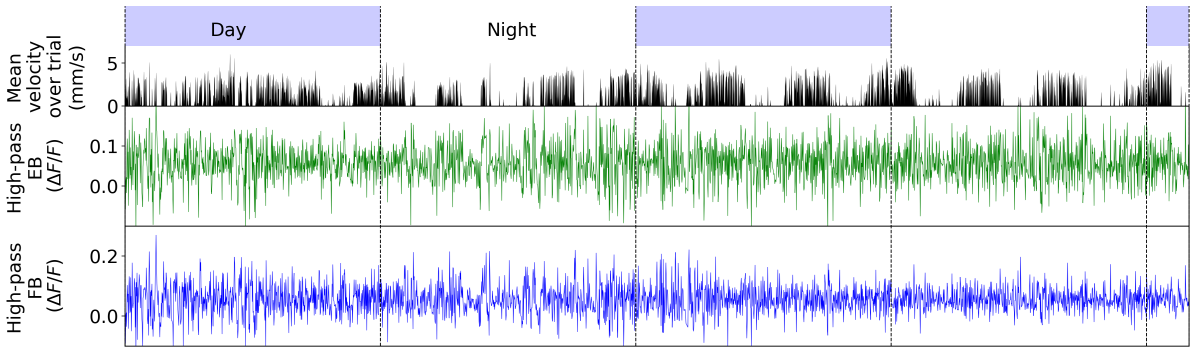

Figure S11. High-pass filtered fluorescence activity in Fig. 1d. **a** Top row shows day and night cycle in VR over time and second row shows mean velocity during recording epoch (1 second). Second and third row show fluorescence signals in the EB and FB, respectively. Fluorescence was filtered with a high-pass filter for periods higher than 0.5 hours. Correlation between mean velocity over trial and high-pass filtered fluorescence is shown in Fig. 3e.

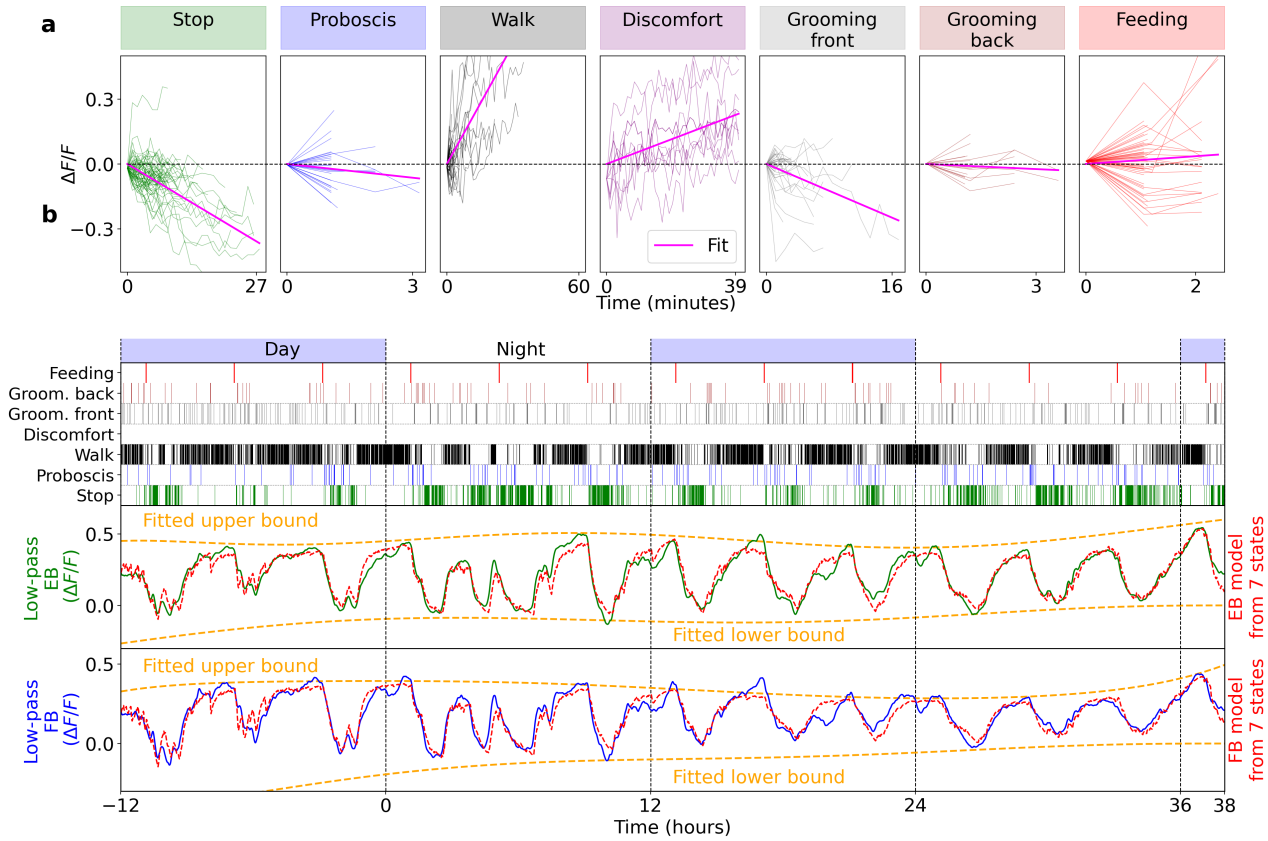

Figure S12. Fitting calcium activity with 7 behavioral states (seven-state model). **a** Determination of sign of weights of each behavior for model fitting. Fluorescence traces performing the respective behavior for at least to consecutive fluorescence recordings (2 minutes, combined across flies, see Methods). Purple shows linear fit, negative slope results in negative weight, and *vice versa*. Flies were often walking fast during feeding, likely resulting in increasing fluorescence. Note that scale on y-axes differs between plots. **b** Model fitting with 7 states. Top: day-night cycle. Second row: classified fly behavior over time. Third row: band-pass filtered activity of glia in the EB (green line); red line shows model fit, orange lines show fitted correction of fluorescence levels. Fourth row: same as third row for FB. **c** Top row: time constants of fitted model for EB (green) and FB (blue) with estimation error. Second row: weight of each behavior as determined in a. **d** Time constants of fitted models for EB (green) and FB (blue) for $N = 6$ flies. Asterisks represent statistical significance in time constants between pairs of behaviors, for p-values lower than 0.05 using t-test (see Extended Data Fig. S13 for a comparison between all pairs of behaviors). **e** Comparison between the 2-state and 7-state models in the EB (left) and FB (right). L2-error between fit and data for $N = 6$ flies.

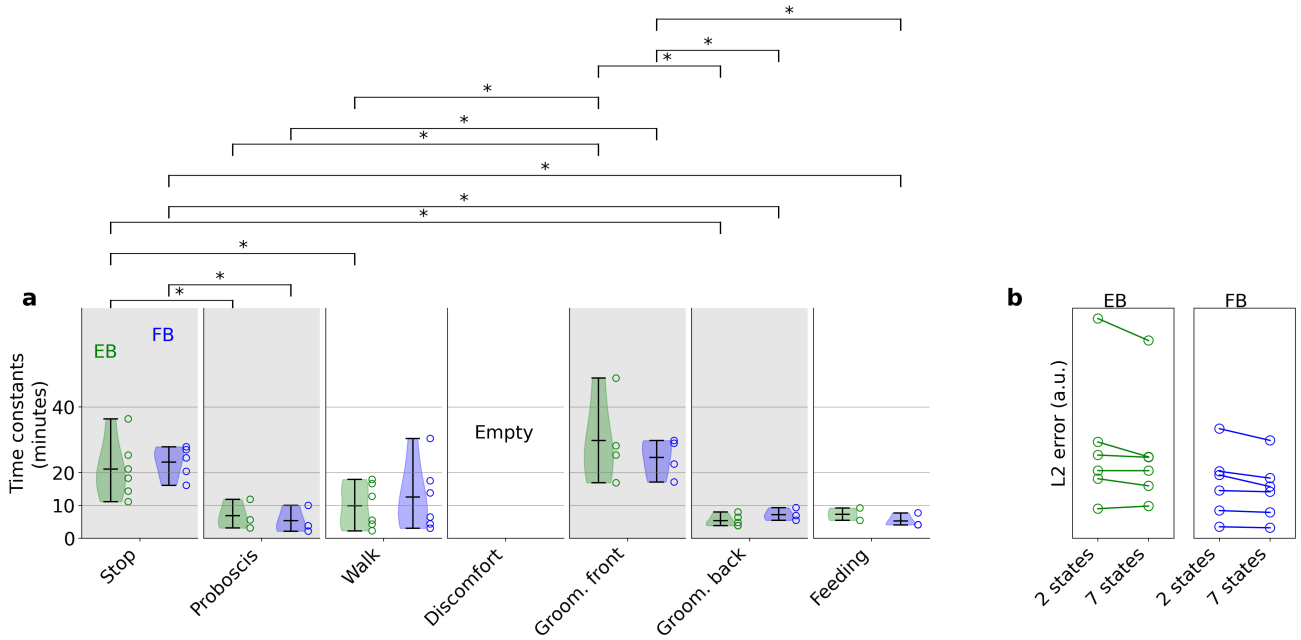

Figure S13. Significance levels for behaviors in 7-state model. Time constants of the 7 classified behaviors fitted in 7-state model for the EB (green) and FB (blue, Fig. S12a). Only time constants with an error of less than 20% were included in the histograms (see Methods). Asterisks include statistical significance between all possible pairs of fitted time constants, based on p-values lower than 0.05 using t-test.

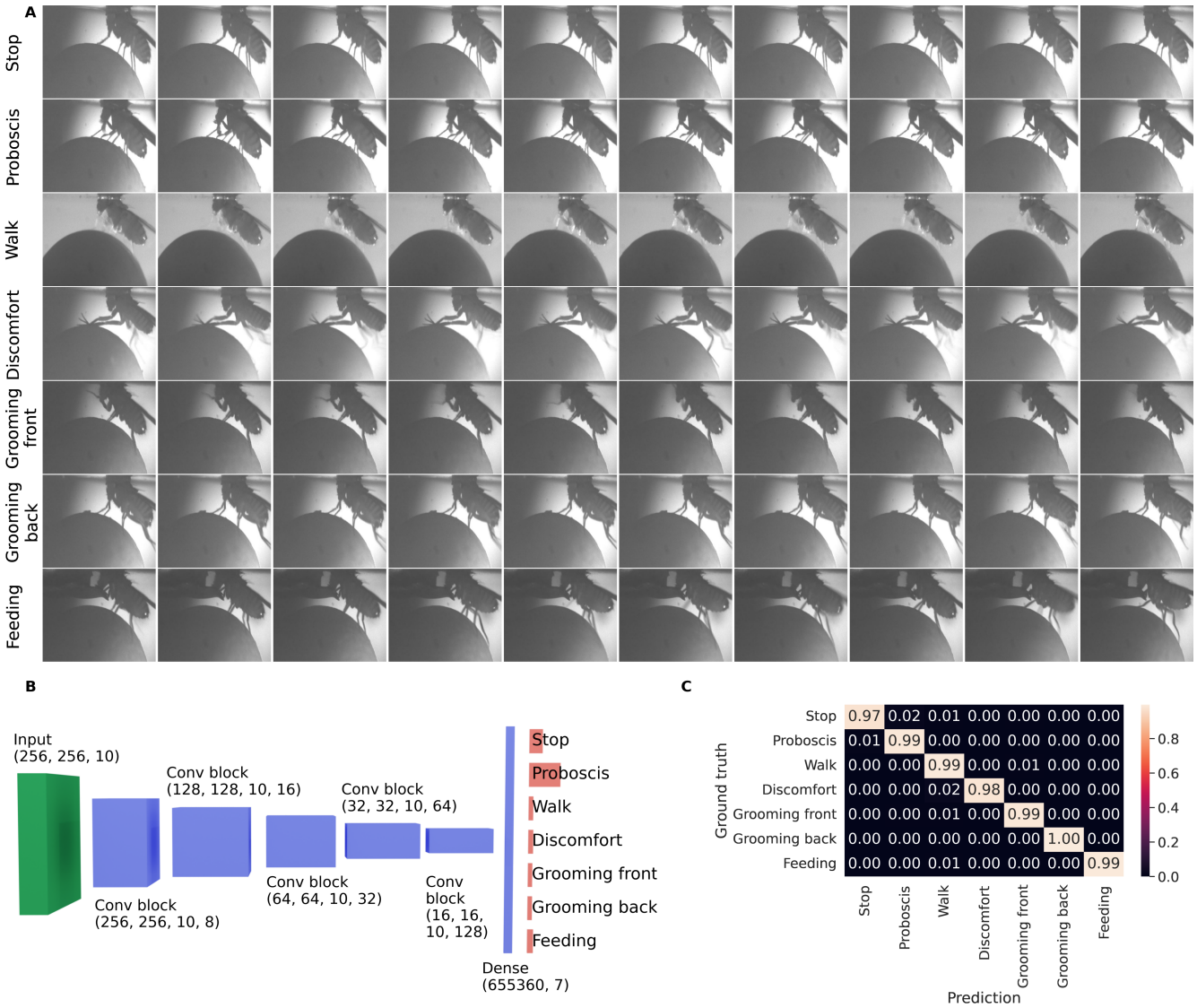

Figure S14. Classification of behavior of the fly on the ball during long-term imaging. **a** A 3D CNN with 10 consecutive frames of images with a side view of the fly on the ball is used to classify 7 different behaviors (y-axis). Each row in the plot corresponds to 10 consecutive frames where the fly performs the labeled behavior. **b** Architecture of the 3D CNN. **c** Confusion matrix for each behavior for prediction of the 3D CNN (x-axis) on a test dataset that was manually labeled (ground truth along y-axis).

Supplementary Video S1. Video for experiment of fly 1. Top: time during experiment. Middle, right: raw imaging data (60 frames or 1 second average in epochs of 1 minute). Rotating blue (during the day) or grey (during the night) arch represents stripe orientation in VR with respect to the fly (the fly's head and abdomen are pointing toward the upper and lower axis of the video, respectively). Right: side view of the fly on the ball. Behavior classification is shown in white in the left corner. The bottom panel shows the velocity of the fly (first row), behavior classification (second row), and glia activity in EB (green) and FB (blue) over time. Grey areas in top and bottom row indicate night (VR display is off). The time of extracted movies in the experiment are shown are indicated by the green bar.

Supplementary Video S2. Same as Supplementary Video S1 for fly 2.

Supplementary Video S3. Same as Supplementary Video S1 for fly 3.

Supplementary Video S4. Same as Supplementary Video S1 for fly 4.

Supplementary Video S5. Same as Supplementary Video S1 for fly 5.

Supplementary Video S6. Same as Supplementary Video S1 for fly 6.

Supplementary Video S7. Classification of fly behavior using the 3D CNN. The video shows different moments where the fly performs different behaviors.

Supplementary Video S8. Example of tracking freely walking flies in optogenetics setup under infrared illumination.